GIA NEWS FROM RESEARCH

The report indicates the status of a research project that is still ongoing within GIA.
Comments on this and other reports and their direction are warmly welcomed as are offers of collaboration.
Contact information can be found in the “about the authors” section on page 40.

# A STUDY OF SAPPHIRE FROM CHANTHABURI, THAILAND AND ITS GEMOLOGICAL CHARACTERISTICS

*Sudarat Saeseaw, Supharart Sangsawong, Wim Vertriest, Ungkhana Atikarnsakul, Victoria Liliane Raynaud-Flattot, Charuwan Khowpong, and Vararut Weeramonkhonlert*

**Figure 1: Rough and facetted sapphires from Thailand. The large facetted stone in the center weighs 8.14 ct. Stone courtesy of Indy Khurana (Khurana Jewels, Bangkok). Photo by Wim Vertriest © GIA.**

## Table of Contents

## PART I: INTODRUCTION TO THAI SAPPHIRE

### 1.1 Thai Sapphire history

Since the second half of the twentieth century, Thailand has played a leading role in the ruby and sapphire industry. Over the last 60 years, the country has established itself as a mining area (mainly in the 1980s), trading center, and treatment hub for many types of gem corundum (Keller 1982, Hughes 2016). Small-scale gemstone mining and trading in Eastern Thailand was described as early as the 15th century (Bauer 1904, Pavitt 1973, Keller 1982). In the late 1890s and early 1900s, the gem mines around Chanthaburi and Trat became more active with investment from foreign companies (Black 1896, Warington Smyth 1898, Bauer 1904). In the 1960s, sapphire mining activity in Thailand increased due to political instability in the neighboring countries of Myanmar and Cambodia, which were also major gem producers (Keller 1982). During the 1980s, Thailand became a significant global sapphire producer with Kanchanaburi as the largest mining area (Kammerling 1990). Since the 1990s, mining has decreased because of mine exhaustion and competition from other deposits (Kammerling 1996). In the early 2000s, sapphire mining in Chanthaburi province picked up because material from this location was very well suited for the newly-developed beryllium-diffusion treatment. The star sapphires from the area often benefit from glass filling techniques (Hughes 2016).

At the time of writing, a dozen mining crews are still working around Chanthaburi, mainly in the Khao Ploy Waen and Bang Kacha areas. Although Thailand has passed its peak as a gemstone mining country, it is still a major center for trading, treatments, cutting, and jewelry manufacturing. The country's two main gem and jewelry industry related areas are Chanthaburi city and the Silom-Charoen Krung area in Bangkok.


Figure 2: Map showing the location of Chanthaburi in the Southeastern part of Thailand, near the Cambodian border.


Figure 3: A satellite image showing the location of Chanthaburi city and the two most active mining areas, just west of the city.

## 1.2 Chanthaburi & Khao Ploy Waen: Mining culture

### 1.2.1 CHANTHABURI TOWN

Figure 4: Sapphire-covered statue of the Virgin Mary in the Chanthaburi Cathedral. Photo by Vincent Pardieu © GIA.

The city of Chanthaburi is a true cultural melting pot. Its long history as a successful port attracted numerous foreign minorities. It is also one of the few parts of Thailand colonized by European nations. From 1893 until 1905, Chanthaburi was under French control. That nation's influences can still be noticed in the city's central cathedral, construction of which started under French control. Apart from Thai and Chinese communities, Chanthaburi hosts a large number of Vietnamese and Shan (also known as Gula) from Myanmar. The Vietnamese community arrived in Chanthaburi after fleeing their homeland. The first wave arrived in the 19th century, when catholic minorities were persecuted during the Chinese occupation. Later waves included refugees fleeing from French Indochina during the interbellum. A last wave of refugees fled from Vietnam to Chanthaburi after the communist victory in 1975. The Burmese community had experience with precious stones from their home country and quickly recognized Chanthaburi's gem potential. Many of these groups included non-Buddhists and many Christians. Some became successful merchants and contributed greatly to the region's wealth. This success is represented by the sapphire-encrusted statue of the Virgin Mary in Chanthaburi cathedral, donated by the local community.

### 1.2.2 KHAO PLOY WAEN

The small hill about 8 km west of Chanthaburi holds great importance to the local gemstone mining community. The name Khao Ploy Waen literally means 'The Hill circled by Gems'. It is the opening in the earth where the gem-bearing basalts reached the surface. The hill itself is composed of basalt and the surrounding lowlands have been covered by flows from its vent. The longest flows moved towards the southeast (Bang Kaja). The hill itself holds great symbolic meaning for the local population, and has never been mined. Mining is only done on the lowest flanks and in the surrounding flatlands. A monastery is located upon its flanks, near the stairs that lead towards the top of the hill. At the very top of the hill, a small pagoda has been constructed. Local miners commonly bring offerings to this pagoda

at the beginning of the mining season or when opening a new pit. Inside a shrine next to the pagoda, a statue of the Hindu deity Ganesha symbolizes the ties this region has with Hindi gem merchants and miners. The wooden statue is accompanied by Ganesha's mount, a mouse, who holds a large gem. The statue used to be decorated with numerous black star sapphires and other gems, but these were brutally carved out and stolen in early 2016.

**Figure 5: Ganesha statue on top of Khao Ploy Waen. Photo by Vincent Pardieu©GIA.**

**Figure 6: A close-up on the decorated Ganesha statue on the top of Khao Ploy Waen in April 2015. Photo by Wim Vertriest©GIA.**

**Figure 7: A close-up on the decorated Ganesha statue on the top of Khao Ploy Waen in March 2016 showing damage caused by removing the gems. Photo by Wim Vertriest©GIA.**

### 1.2.3 REHABILITATION OF MINES

The stairs to the top of Khao Ploy Waen offer great views over the surrounding area. After regular visits to the area over the span of several years, it became clear to the authors that this is a very dynamic environment where land use changes frequently between agriculture and gem mining.

**Figure 8: View from the top of Khao Ploy Waen towards the northeast. The landscape is dominated by fruit plantations, with some sapphire mines in between the green patches. Photo by Wim Vertriest © GIA.**

North and East of Khao Ploy Waen, the land is dominated by plantations, (including bananas, durian, guava, papaya, dragon fruit, and rubber), while the southern side gives a wide view of the many seafood farms near the coast. The whole area is very fertile (volcanic derived soils are rich in minerals and retain water well) and thus extremely well suited for farming of tropical fruits. Dotted between these farms are the sapphire mines. The whole area is underlain by gem bearing basalts, so the sapphires can be found over a large area. Mining is usually done on farmland. At the end of a fruit farm's lifetime, the land is cleared and the farmer goes into a joint venture with a miner (or group of miners). They make a financial arrangement, usually with the farmer providing the land and the miner providing mining equipment and expertise. Over a certain timespan, the plot of land is mined. When the ground is washed, the pits are filled and usually no visible sign of the mines remains in the landscape. When mining is finished, the miner rehabilitates the land, turning it into farms again. Usually the first stage involves planting banana trees, a crop that is traditionally used to condition the soil. Later, other trees such as papaya or durian are added to the plantations. The mining leaves no lasting marks on the environment, since the land is restored to plantations. Over the years, we have seen the landscape change. At the same place, we have seen a fruit plantation which was turned into a sapphire mine. Visiting the same location a few years later, it was covered in young banana trees.

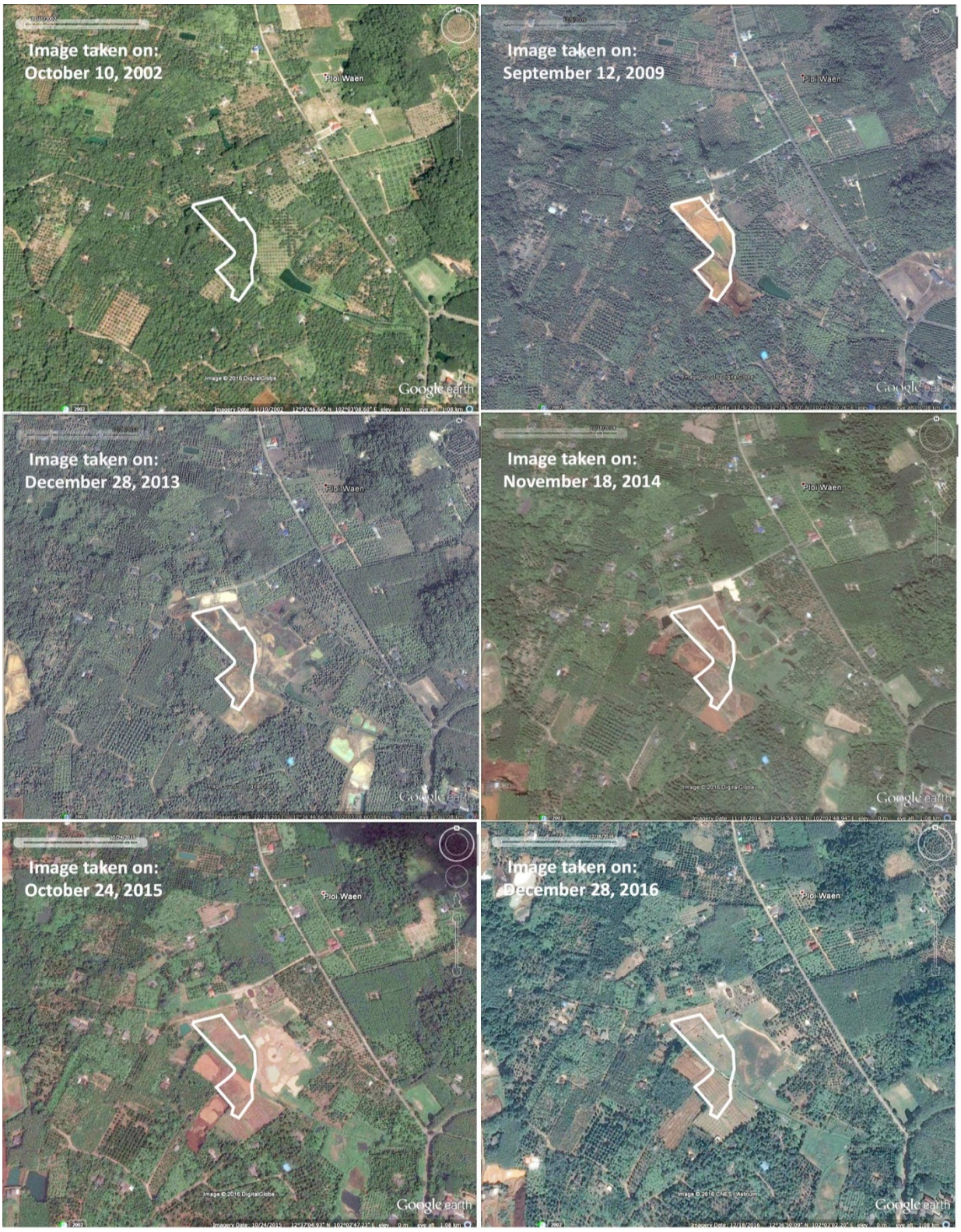


**Figure 9: Series of satellite images showing an example of the construction, development and rehabilitation of a sapphire mine near Khao Ploy Waen, Thailand. We can clearly see that between 2002 and 2009 the highlighted area is developed as a mine. Overtime it expands and by the end of 2016, the original highlighted area is once again a plantation. Around Khao Ploy Waen, many of these examples can be found (e.g. the southeastern corner of the images).**

### 1.2.4 MR WUYI'S MINE

All of the samples used in this study were mined by Mr. Samran 'Wuyi' Raktantikiet and his partner, Mr. Kajorn Kitnawa. Wuyi is a farmer who owns a plot of land in the lower slope at the eastern side of Khao Ploy Waen. He lives with his wife in a house surrounded by plantations. A small part of the area has been cleared and is being mined. Mining gear and expertise is supplied by his partner, who also has several commercial contacts in town. Mr. Wuyi's mine is one of the smallest operations in the area, but he is very friendly and gladly welcomes visitors. Many gemological institutes, universities and private travelers have visited him. The mining duo allows visitors to get some practical experience mining and cleaning the jig. Their main production consists of black star sapphires, complemented by blue-green-yellow sapphires. They also recover some deep-red garnet, which can be big enough for faceting.

**Figure 10: Mr. Samran 'Wuyi' Raktantikiet (wearing the hat) and his partner, Mr. Kajorn Kitnawa at their mine. Photos by Victoria Raynaud © GIA.**

## 1.3 Geology of the Chantaburi gem deposits

The gem deposits of Chanthaburi and Trat are associated with alkali basalts (Keller 1982). These are basalts that form at great depths, usually assumed to be in the mantle, near the transition zone with the crust. Southeast Asia hosts multiple alkali-basalt extrusions that are of Cenozoic (Tertiary) age. These types of deposits mainly produce BGY (blue-green-yellow) sapphires (Levinson and Cook 1994). In Chanthaburi, black star sapphires are also found.

The gems occur in these basalts as xenocrysts ( Figure 11) (Levinson and Cook 1994, Sutherland 1998, Saminpanya 2011). This means that they have not formed in the basalt, but were picked up by the basalt and transported to the surface. The three main arguments for this conclusion are:

1. Experiments to crystallize corundum from a melt of similar composition to alkali basalt have never been successful.
2. The corundum never shows a perfect crystal habit, it is always rounded (even when found in the basalt) and shows etching and resorption, indicating the basalt has started to consume or dissolve the corundum because it is unstable in the basalt during emplacement.
3. Several inclusions in basalt-related rubies and sapphires are impossible to form in alkali basalts.

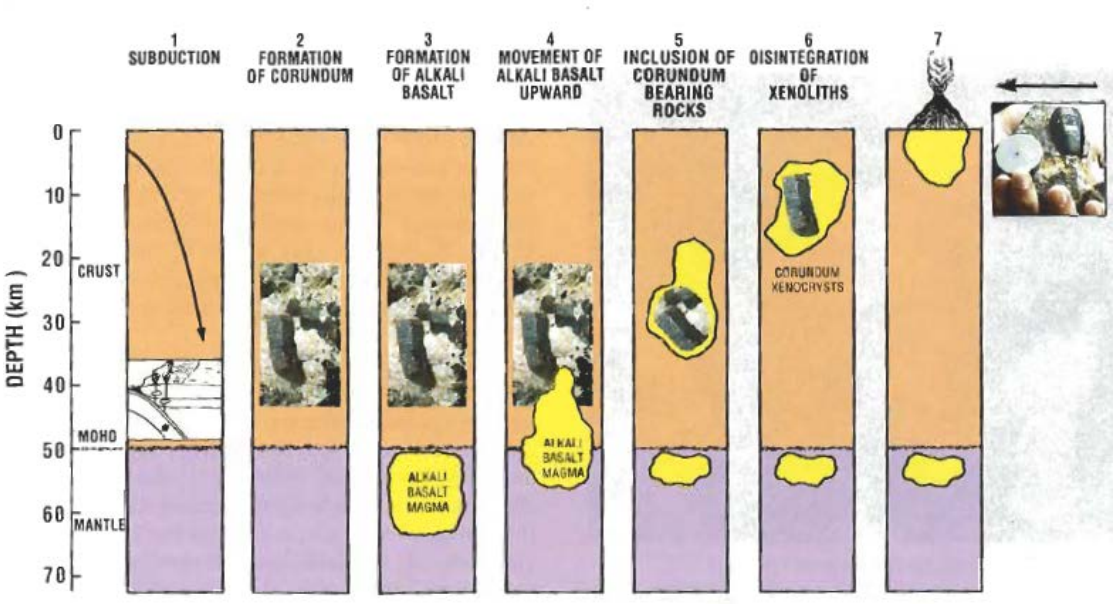


Figure 11: Visualization of the geological process behind basalt-related gem deposits (Levinson and Cook 1994).

**Basaltic versus Basalt-related:**

The term 'basaltic' means that the feature described was formed in the basalt. Levinson & Cook (1994) give sufficient arguments that the ruby and sapphires found in association with basalt did not form in the basalt. Thus they are not basaltic in origin!

In the authors' opinion, it is more correct to refer to these gems as **basalt-related or basalt-hosted**.

Due to Thailand's hot and humid climate, the alkali basalt weathers very quickly. During the weathering process, the more stable minerals are liberated from their basalt matrix. These are mainly corundum, garnet, zircon and large clinopyroxenes. The basalt matrix is turned into a reddish mud (Keller 1982).

The deposits around Khao Ploy Waen are eluvial (Figure 12). This means that the sapphires have not been transported by water. However, the climatic conditions have caused the hard basalt to weather and turn into soft, red mud. The gems are still in the same place as the basalt deposited them (yellow arrow), but the original host rock has completely disintegrated. Sometimes basalt-flows have been covered by marine sediments which have to be removed before miners can access the weathered basalt that hosts the gems (Bang Kacha, purple arrow).

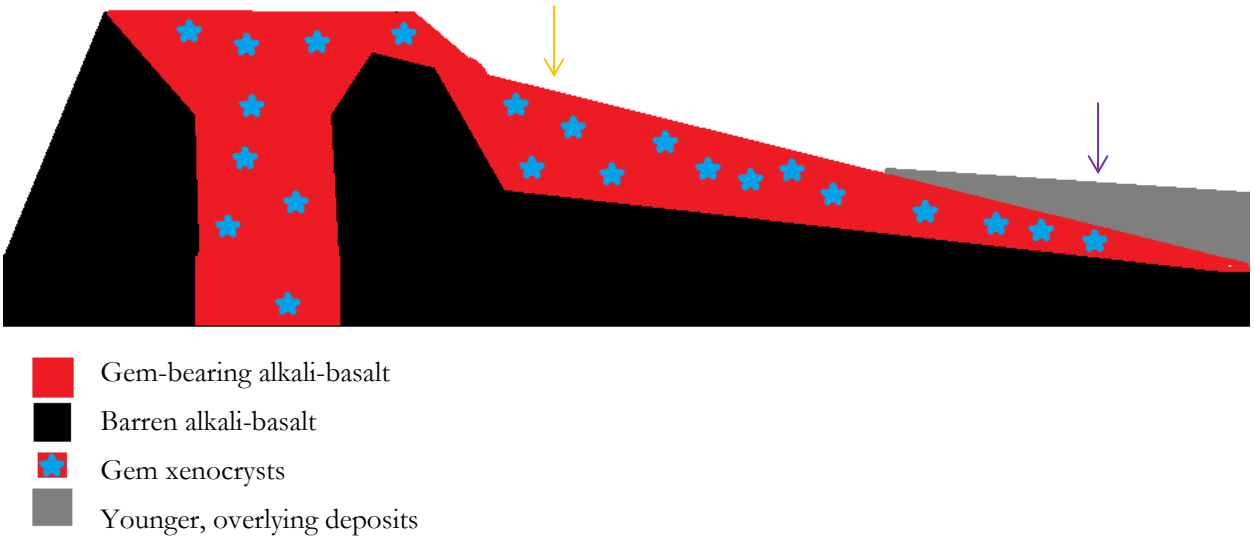


**Figure 12: Sketch showing the occurrence of sapphires in weathered basalts around Khao Ploy Waen.**

## 1.4 Mining Techniques

Around Chanthaburi, most of the mines are mechanized nowadays. The operations are concentrated around Khao Ploy Waen, which is the volcanic hill where the alkali-basalt reached the surface, and in the Bang Kacha area to the east of Khao Ploy Waen.

Small scale miners dig a pit and pile up all the excavated ground next to it. They place a small pulsating jig between the pit and the pile and start washing the entire pile through the jig. The rejects, finest fractions and light materials are all dumped back into the pit. A pump cycles the water from the pit to a high-pressure water jet that is used to liquefy the excavated ground to make sure it can easily flow to the jig. Periodically, they stop the washing to clean the jigs and sort the concentrate of heavy minerals.

**Figure 13: View of Mr. Wuyi's mine near Khao Ploy Waen. The material is washed from the pile on the right, through the jig in the center into the pit on the left side. Photo by Vincent Pardieu © GIA.**

Other mines operate on a larger scale. In some cases, overburden (ground that does not contain gems) has to be removed first. Miners often use excavators to feed the mud directly into washing installations. The first part of the equipment consists of revolving screens that are equipped with high-pressure water jets to break up clay balls and sort out stones that are oversized. The remaining concentrate of loose pebbles is pumped to a pulsating jig where it is collected. Periodically (usually at the end of the day), the jig is opened and cleared of valuable stones.

**Figure 14: An excavator digging sapphire-bearing ground near Bang Kaja. The excavator dumps material in the jig's feed bucket, where it goes into the revolving screen. The washed gravels move towards the gravel pump (at the base of the tripod). Note the contrast between the gray marine clay and the red weathered basalt in the background. Photo by Wim Vertriest © GIA.**

## PART II: MATERIALS AND METHODS

### 2.1 Sample Fabrication:

Fifty-nine (59) samples were selected to study the characteristics of blue sapphires from Chanthaburi, Thailand. According to the GIA Field Gemology sample classification system, these samples are type B, C and D-type.

- B-type: Mining was witnessed by the gemologist, usually collected from the jig.
- C-type: Sample was collected from the miner at the mine, but without witnessing the mining.
- D-type: Sample was collected from the miner, but not at the mine (e.g. at the miner's house).

Color ranged from **greenish blue to blue** when viewing perpendicular to the c-axis direction, which is only the O-ray direction, whereas **yellowish green to blue** color is seen when viewing parallel to the c-axis direction, which is O+E ray direction. Samples were fabricated for two different purposes:

i) Three (3) samples that had sufficiently clean areas were fabricated with windows parallel to c-axis for UV-Vis-NIR spectroscopy and chemistry, Table 1.

ii) Fifty-seven (56) samples were fabricated with at least one window for inclusion photography, FTIR, and chemistry, Figure 15.

**Table 1: Details of the three sapphires from Chanthaburi, Thailand for UV-Vis-NIR and FTIR spectroscopy, and chemical analysis.**

| GIA Reference # | Wafer Plane orientation | Wafer path length (mm.) | Image O+E ray color | Image through a dichroscope (color) |
|---|---|---|---|---|
| 6688**4000**2 | Parallel to c-axis | 1.065 |  Blue |  Blue/ Bluish Green |
| 10030993**5040** | Parallel to c-axis | 0.259 |  Yellow |  Yellow |
| 10030993**5039** | Parallel to c-axis | 1.899 |  Greenish blue |  Blue/ Bluish Green |

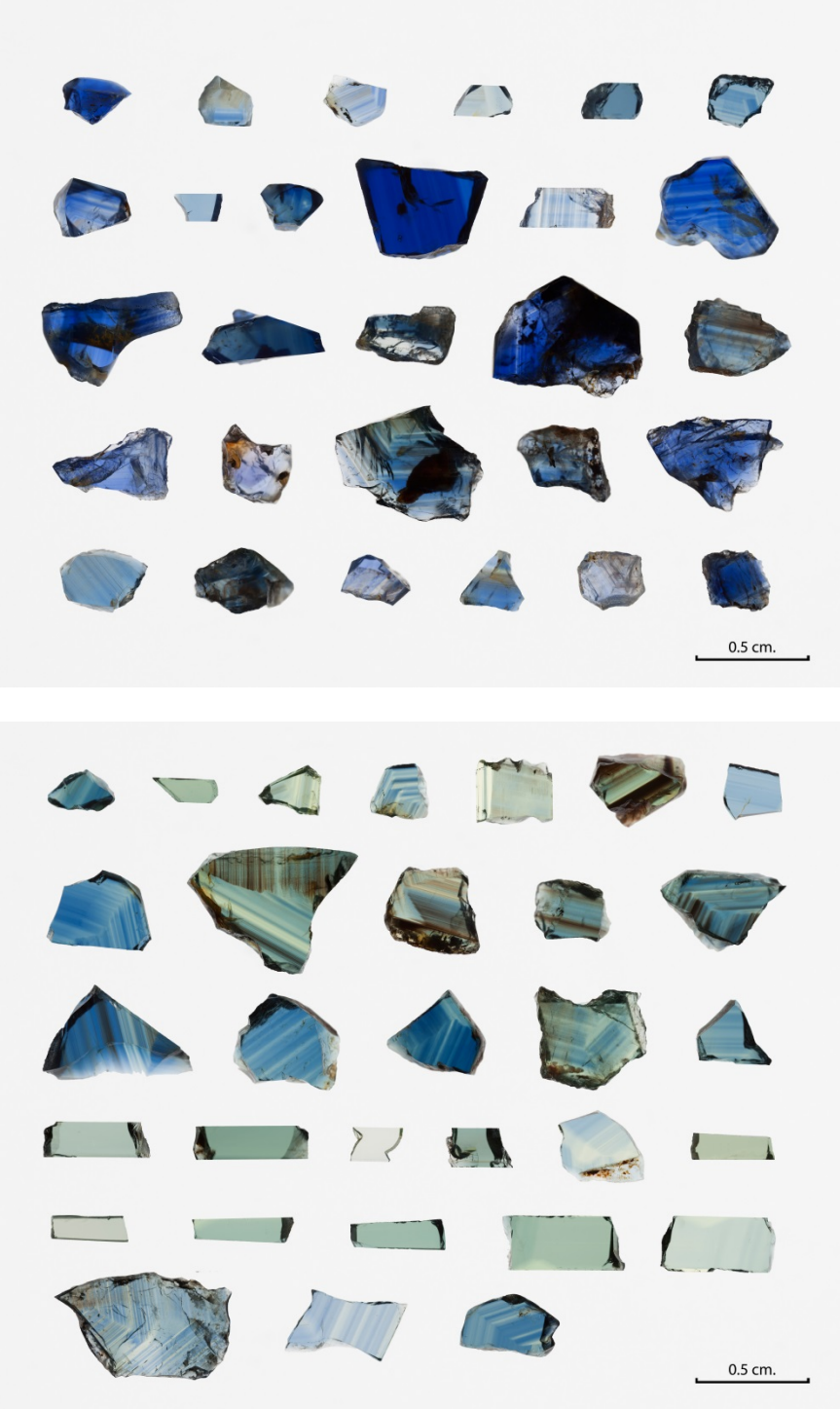


**Figure 15: Blue (top) and greenish blue (bottom) sapphires from Chanthaburi-Trat region, Thailand. The photos were color calibrated using transmitted light. Photos: S. Engniwat © GIA.**

## 2.2 Instrumentation:

### 2.2.1 SAMPLE PHOTOGRAPHY

A Canon EOS 5D camera, with a Canon Macro MP-E 65 mm lens adapted to a camera stand, was used to document the color of the samples. In order to produce consistent results for each sample, the photographs were taken under exactly the same lighting conditions, with the reference samples being placed in a Logan Electric Tru-View 810 Color Corrected Light Box (5000 K lamp). A neutral density filter was used to calibrate the camera light box combination to produce a neutral gray. High-resolution reference photographs were then collected using transmitted light. The color of the sample with polarizer aligned perpendicular to c-axis or 0° sample is the color produced by O-ray only whereas sample with polarized aligned parallel to c-axis direction or 90° sample is the color produced by O + E-ray. Photomicrographs of internal features were captured at different magnifications with a Nikon SMZ 18 system and a Nikon SMZ 1500 system using darkfield, brightfield, diffused and oblique illumination, together with a fiber-optic light source when necessary. It should be noted that magnification power of the microscope was taken into consideration when calculating the field of view (FOV) information in the captions.

### 2.2.2 UV-VIS-NIR SPECTROSCOPY

Ultraviolet-visible-near infrared (UV-Vis-NIR) spectra were collected with a Hitachi U-2910 spectrophotometer specially modified at GIA to include a rotatable polarizer to allow the separate collection of both the ordinary (O-) and extraordinary (E-) rays. A wavelength resolution of 1.5 nm was used. The spectra obtained were corrected by calculating the reflection loss from the index of refraction data and the data was converted to show their absorption coefficients ($\alpha$,$cm^{-1}$) using $\alpha = 2.303A/d$, where *A* is absorbance and *d* is the path length in centimeters.

### 2.2.3 FOURIER TRANSFORM INFRARED ABSORPTION (FTIR) SPECTROSCOPY

FTIR spectroscopy was performed using a Thermo Nicolet 6700 FTIR spectrometer equipped with an XT-KBr beam splitter and a mercury-cadmium-telluride (MCT) detector operating with a 4× beam condenser accessory. Resolution was set at 4 $cm^{-1}$ with 1.928 $cm^{-1}$ data spacing. The spectra obtained were converted to be absorption coefficients ($\alpha$, $cm^{-1}$) using $\alpha = 2.303A/d$.

### 2.2.4 RAMAN SPECTROSCOPY

To identify mineral inclusions, Raman spectra were obtained using a Renishaw inVia Raman microscope fitted with a 514 nm argon-ion laser. The spectra were collected in the range of 100 and 1500 $cm^{-1}$. The accumulation was set at a minimum of 5 until the signal to noise ratio of the spectra was adequate. The calibration was performed using the 520.5 $cm^{-1}$ line of a silicon wafer. In all cases, the RRUFF database was used as a reference when identifying inclusions. Spectral comparisons were performed using Renishaw Wire (version 3.4) and/or Thermo Galactic 'Spectra ID' (version 3.02) software.

### 2.2.5 LASER ABLATION-INDUCTIVELY COUPLED PLASMA-MASS SPECTROMETRY (LA-ICP-MS)

Chemical analysis was carried out using LA-ICP-MS technology with a Thermo Fisher Scientific iCAP Q Induced Coupled Plasma-Mass Spectrometer (ICP-MS) coupled with a Q-switched Nd:YAG Laser Ablation (LA) device operating at a wavelength of 213 nm. Laser conditions used were 55 µm diameter laser spots, a fluency of around 10 J/cm$^2$, and a 15 Hz repetition rate. Twelve spots were analyzed on each wafer. ICP-MS was operated using the forward power at ~ 1350 W and the typical nebulizer gas flow at ~ 1.00 L/min. Helium was used as the carrier gas in the laser ablation unit and the flow rate was set at ~ 0.60 L/min. The criteria for the alignment and tuning sequence were to maximize Be counts and to keep the ThO/Th ratio below 2%. A special set of doped synthetic corundum standards including Be, Mg, Ti, V, Cr, Fe, and Ga were used for quantitative analysis. All elemental measurements were normalized to Al as the internal elemental standard, (Al=529,200 ppmw). This value approximates to the chemical composition of corundum.

## PART III: RESULTS AND DISCUSSION

## 3.1 The internal world of blue sapphires from Thailand

Most of the samples have a greenish-blue to blue color. Refractive index ranged from 1.760 ±0.001 to 1.770±0.002, and specific gravity was about 4.0±0.3. Due to the samples' high Fe content, we observed clear absorption lines at 450 and 460 nm with a handheld diffraction-grating spectroscope. None of the stones showed a reaction under long- and short-wave UV radiation.

Microscope examination revealed most Thai sapphires contained angular growth structures, needles, and particles, which may or may not be associated with color zoning (Figure 16 to Figure 25). Distinctive brownish and blue color zoning in Thai sapphire is quite conspicuous. The brownish zones are related to tiny rutile inclusions. The silk in greenish blue sapphires has more 'platy' appearance (Figure 26 to Figure 31). Milky thin films occurring between tiny particle bands or clouds were also observed in Thai sapphires (Figure 35 to Figure 37). A few stones contained intersecting needles (Figure 32 and Figure 33) and bands of very fine minute particles (Figure 38 and Figure 38). Iridescent fluid inclusions in fingerprints that often formed with negative crystals or feldspar, were commonly detected (Figure 43 to Figure 51). In addition, Thai sapphires contain a variety of mineral inclusions, such as plagioclase feldspar, zircon, pyrochlore, monazite, mica, and molybdenyte (Figure 52 to Figure 63). Of these, feldspar was the most common and frequently associated with partially-healed fissures.

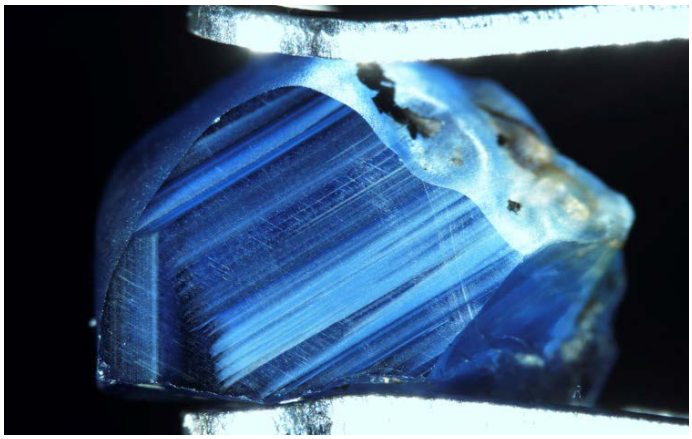

Figure 16: Angular bands of tiny particles forming along growth features in GIA reference sample 668839902. Darkfield and fiber-optic illumination. FOV 7.2 mm. Photo: V. Raynaud © GIA.

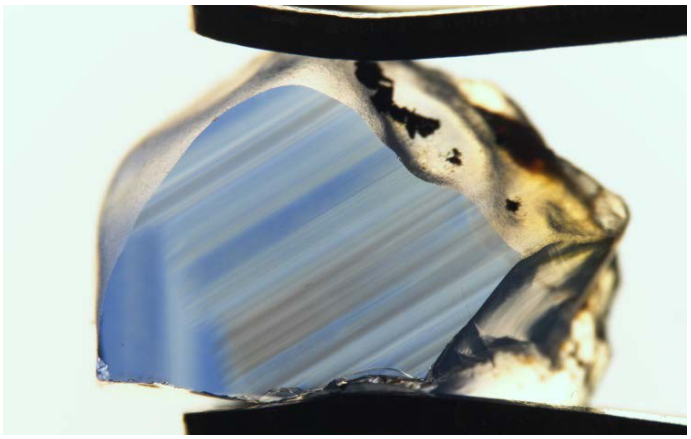

Figure 17: In diffused illumination the distinctive tiny particles are associated with brownish zoned whereas blue color zoning are particle free in GIA reference sample 668839902. FOV 7.2 mm. Photo: V. Raynaud © GIA.

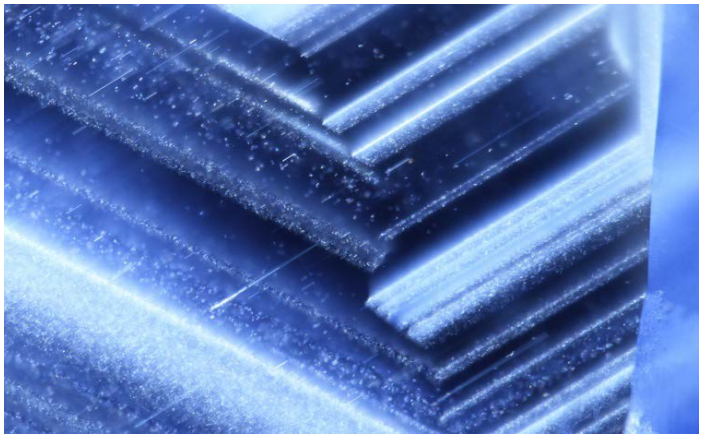

Figure 18: Distinct bands of tiny particles along with blue color zoning in GIA reference sample 668841902. Darkfield and fiber-optic illumination. FOV 1.75 mm. Photo: V. Raynaud © GIA.

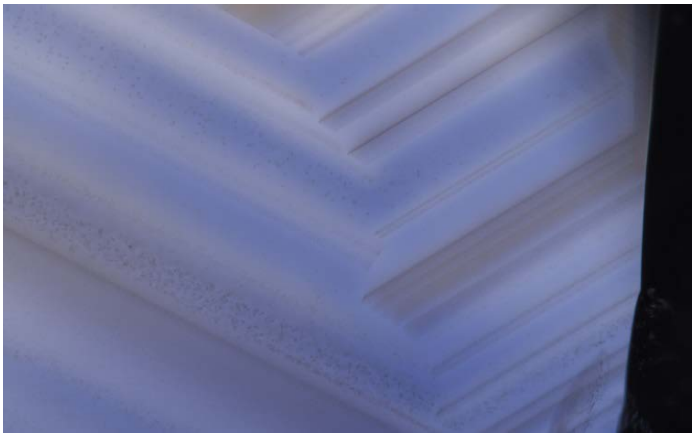

Figure 19: When correctly illuminated, the areas with highest particle density appear brownish in GIA reference sample 668841902. Diffused illumination. FOV 1.75 mm. Photo: V. Raynaud © GIA.

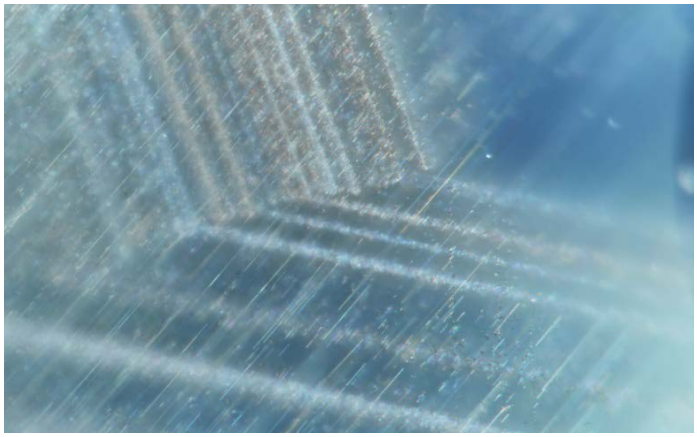

Figure 20: Angular bands of brownish particles associated with short rutile needles in GIA reference sample 668839802. Darkfield and fiber-optic illumination. FOV 1.2 mm. Photo: V. Raynaud © GIA.

Figure 21: Under diffused illumination, the angular bands of brownish particles clearly contrast with the particle-free areas in GIA reference sample 668839802. FOV 1.2 mm. Photo: V. Raynaud © GIA.

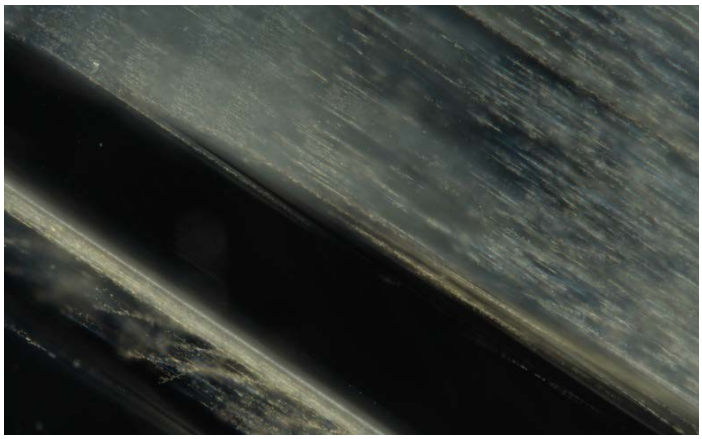

Figure 22: Bands of brownish particles associated blue zoning in GIA reference sample 668839802. Darkfield and fiber-optic illumination. FOV 1.2 mm. Photo: V. Raynaud © GIA.

Figure 23: Under diffused illumination, bands of brownish particles clearly contrast with the particle-free areas in GIA reference sample 668839802. FOV 1.2 mm. Photo: V. Raynaud © GIA.

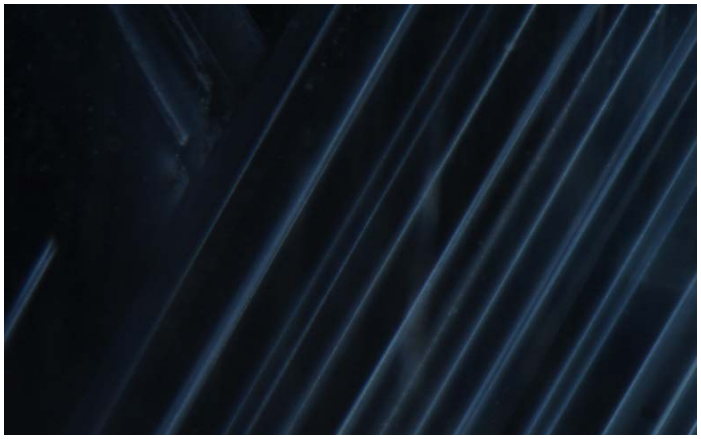

Figure 24: Bands of minute particles in GIA reference sample 668841802. Darkfield and fiber-optic illumination. FOV 1.44 mm. Photo: C. Khowpong© GIA.

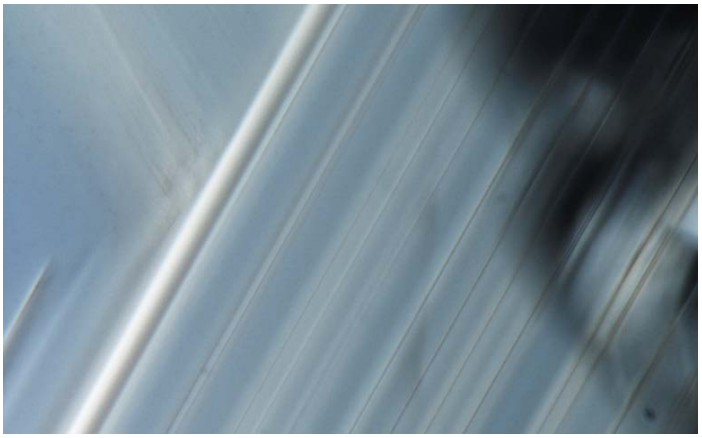

Figure 25: Bands of minute particles appear brownish under diffused illumination in GIA reference sample 668841802. FOV 1.44 mm. Photo: C. Khowpong© GIA.

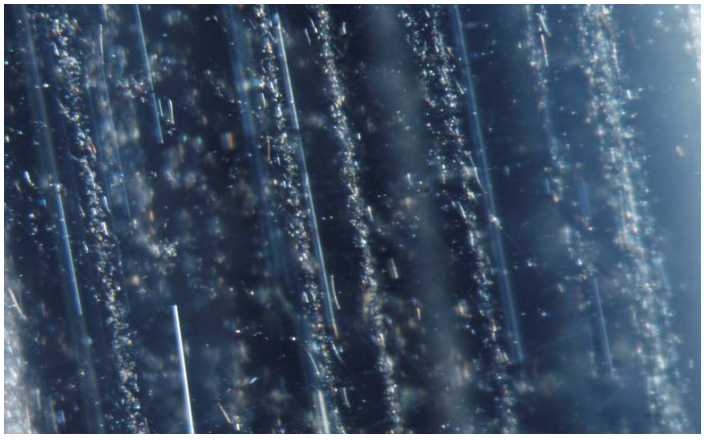

Figure 26: Platy brownish needles in GIA reference sample 100305161818. Darkfield and fiber-optic illumination. FOV 8.2 mm. Photo: V. Raynaud © GIA.

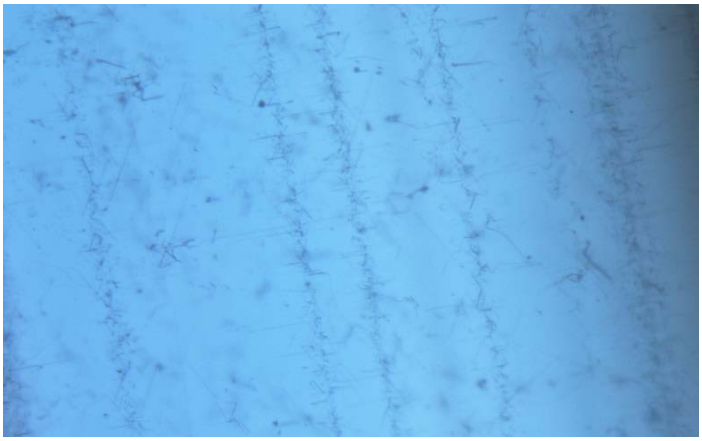

Figure 27: Platy brownish needles stand out under diffused illumination in GIA reference sample 100305161818. FOV 8.2 mm. Photo: V. Raynaud © GIA.

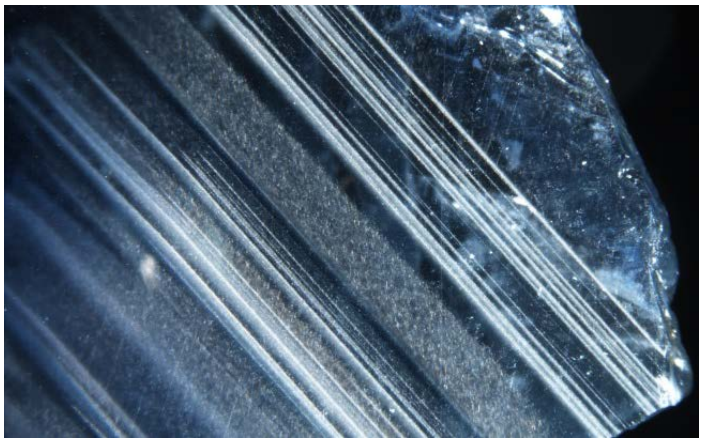

Figure 28: Wide and narrow bands of particles in GIA reference sample 100322689758. Darkfield and fiber-optic illumination. FOV 4 mm. Photo: C. Khowpong © GIA.

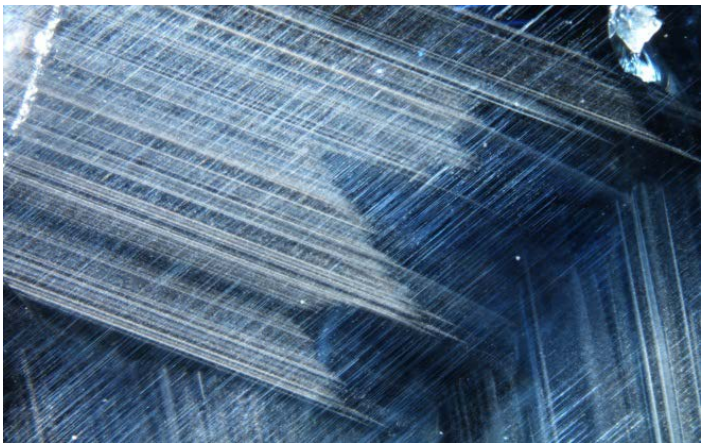

Figure 29: Angular edge bands of needles in GIA reference sample 100322689758. Darkfield and fiber-optic illumination. FOV 8.2 mm. Photo: C. Khowpong © GIA.

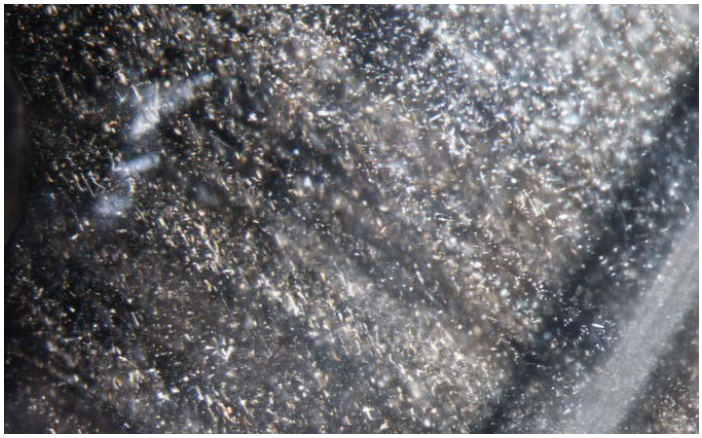

Figure 30: Reflective irregular rutile needles in GIA reference sample 100322689764. Darkfield and fiber-optic illumination. FOV 1.3 mm. Photo: C. Khowpong © GIA.

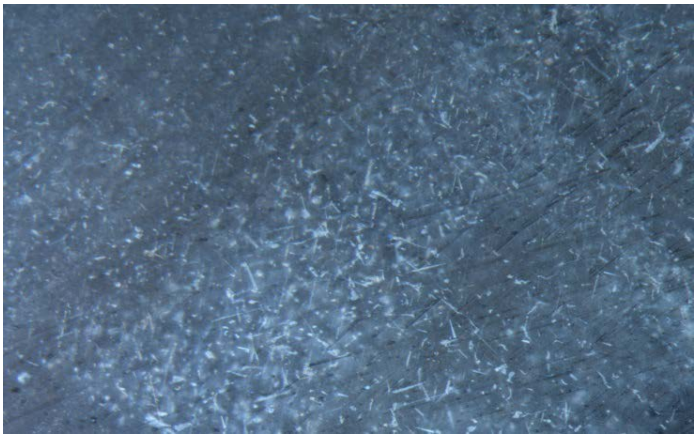

Figure 31: Platy brownish needles in GIA reference sample 100322689755. Darkfield and fiber-optic illumination. FOV 1 mm. Photo: C. Khowpong © GIA.

Figure 32: Intersecting needles in GIA reference sample 100305161405. Darkfield and fiber-optic illumination. FOV 2.7 mm. Photo: C. Khowpong © GIA.

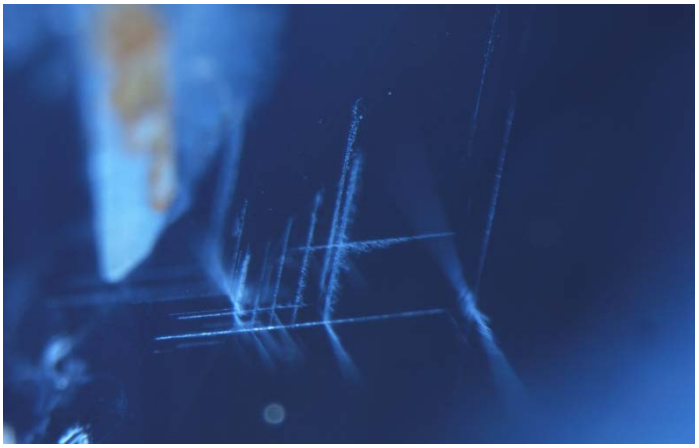

Figure 33: Intersecting needles in GIA reference sample 100305161181. Darkfield and fiber-optic illumination. FOV 1.6 mm. Photo: V. Raynaud © GIA.

Figure 34: Irregular rutile needles and reflective fluid inclusions in GIA reference sample 100322689760. Darkfield and fiber-optic illumination. FOV 2.7 mm. Photo: C. Khowpong © GIA.

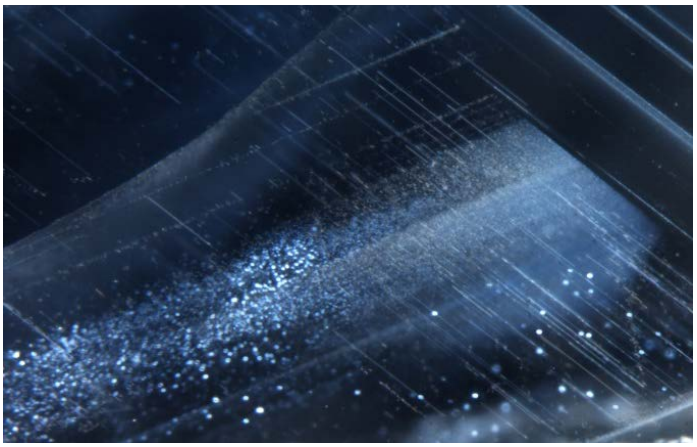

Figure 35: Rutile needles associated with milky thin films in GIA reference sample 100322689760. Darkfield and fiber-optic illumination. FOV 2 mm. Photo: C. Khowpong © GIA.

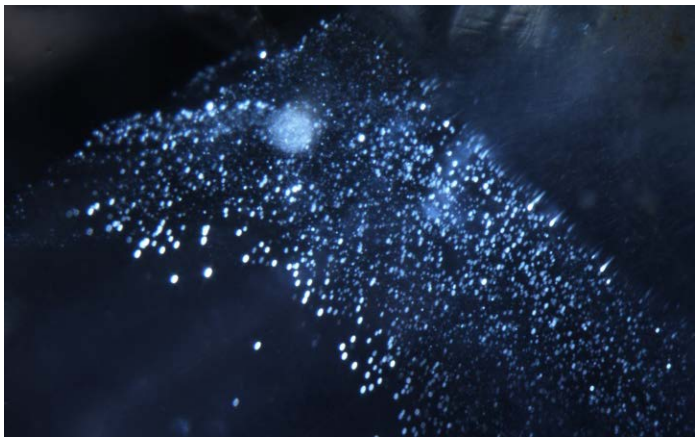

Figure 36: Reflective thin films in GIA reference sample 100322689757. Darkfield and fiber-optic illumination. FOV 2 mm. Photo: C. Khowpong © GIA.

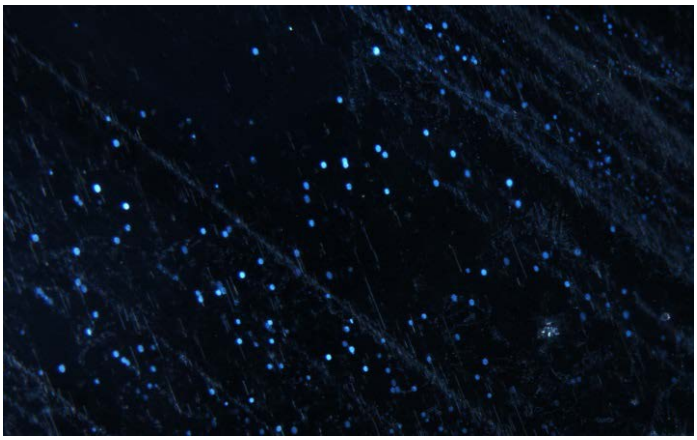

Figure 37: Scattered thin films and rutile needles in GIA reference sample 100322689767. Darkfield and fiber-optic illumination. FOV 2 mm. Photo: C. Khowpong © GIA.

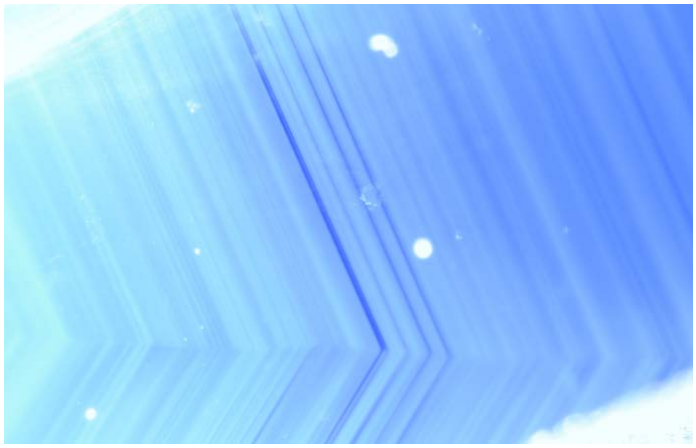

Figure 38: Angular of minute particles in GIA reference sample 100309935275. Darkfield and fiber-optic illumination. FOV 3.1 mm. Photo: V. Raynaud © GIA.

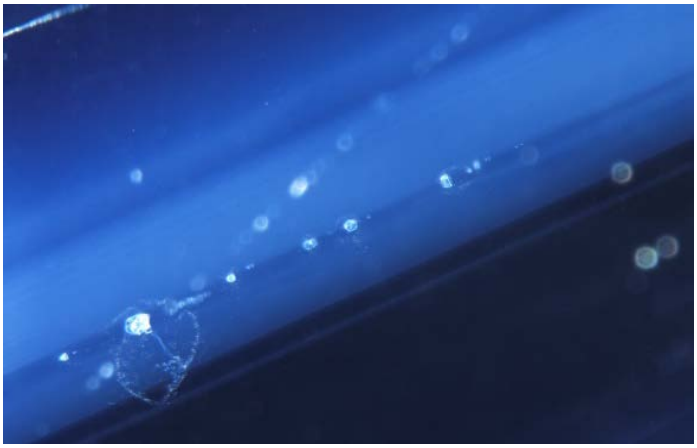

Figure 39: Bands of minute particles and crystals with tension halos in GIA reference sample 100305161181. Darkfield and fiber-optic illumination. FOV 1.3 mm. Photo: V. Raynaud © GIA.

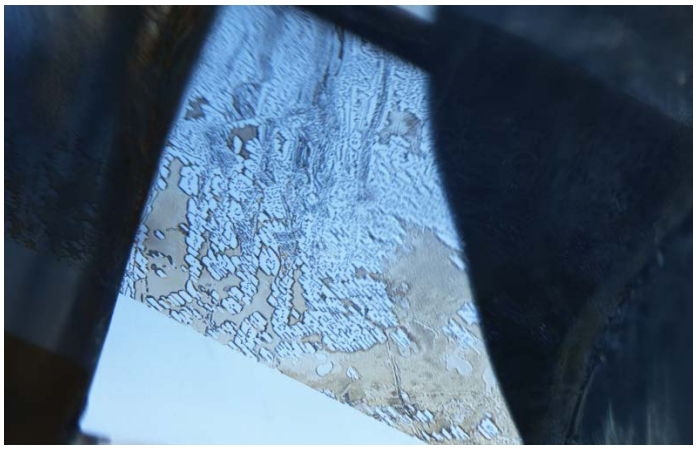

Figure 40: Naturally healed fissures in GIA reference sample 100305161408. Brightfield illumination. FOV 2.4 mm. Photo: V. Raynaud © GIA.

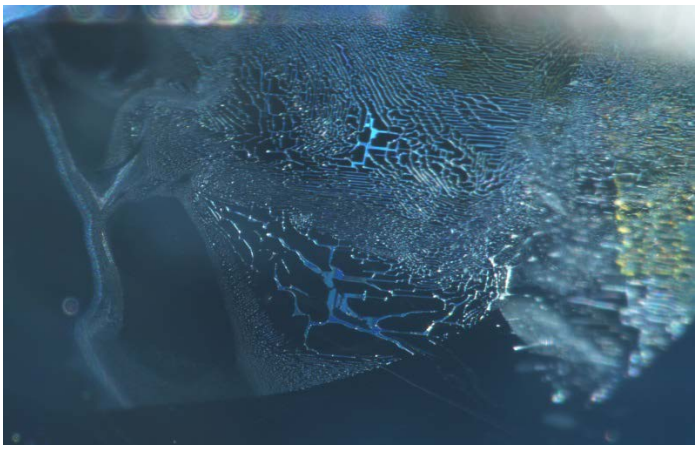

Figure 41: Naturally healed fissures in GIA reference sample 668840002. Darkfield and fiber-optic illumination. FOV 1.4 mm. Photo: V. Raynaud © GIA.

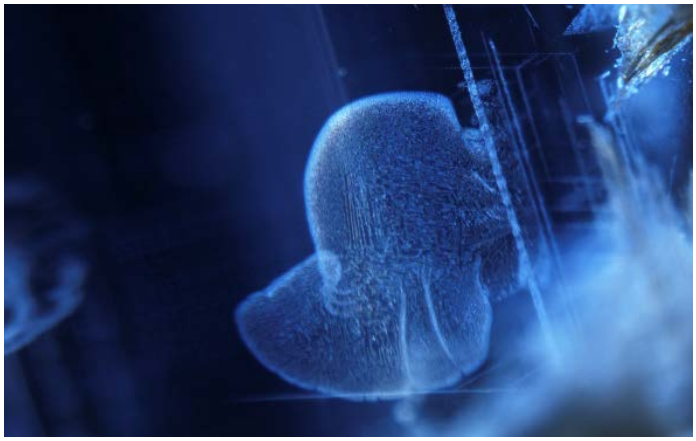

Figure 42: Naturally healed fissures and intersecting needles in GIA reference sample 100305161181. Darkfield and fiber-optic illumination. FOV 2.7 mm. Photo: V. Raynaud © GIA.

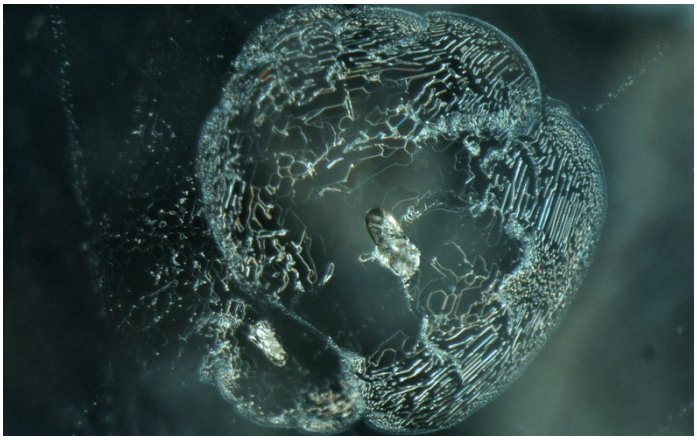

Figure 43: Unidentified crystal associated with naturally healed fissures and intersecting needles in GIA reference sample 100309934721. Darkfield and fiber-optic illumination. FOV 1.4 mm. Photo: V. Raynaud © GIA.

Figure 44: Several naturally healed fractures and some associated with feldspar (identified by Raman) in GIA reference sample 100309934721. Darkfield and fiber-optic illumination. FOV 1.4 mm. Photo: V. Raynaud © GIA.

Figure 45: Crystals associated with naturally healed fractures in GIA reference sample 668839202. Darkfield and fiber-optic illumination. FOV 1.1mm. Photo: S. Sangsawong © GIA.

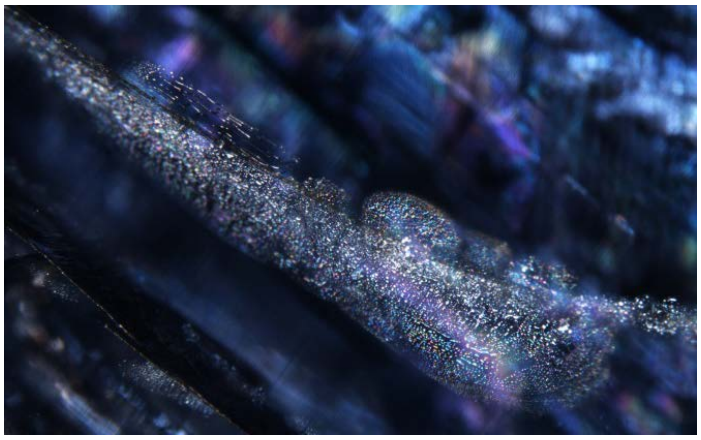

Figure 46: Naturally-healed fractures in GIA reference sample 100322689765. Darkfield and fiber-optic illumination. FOV 2.7 mm. Photo: C. Khowpong © GIA.

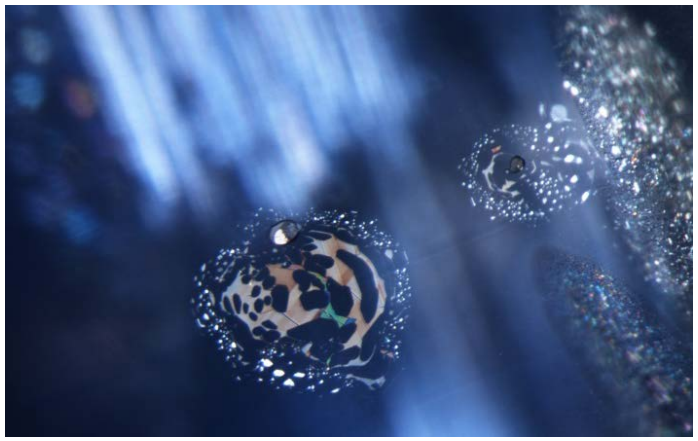

Figure 47: Large decrepitation disc (stress fracture) surrounded by feldspar crystals in GIA reference sample 100322689765. They are not the result of heat treatment. Darkfield and fiber-optic illumination. FOV 0.8 mm. Photo: C. Khowpong © GIA.

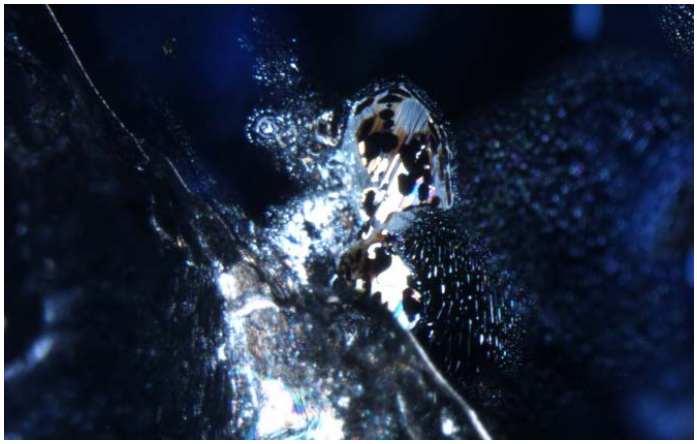

Figure 48: Group of iridescent naturally-healed fractures in GIA reference sample 100322689752 Darkfield and fiber-optic illumination. FOV 1.3 mm. Photo: C. Khowpong © GIA.

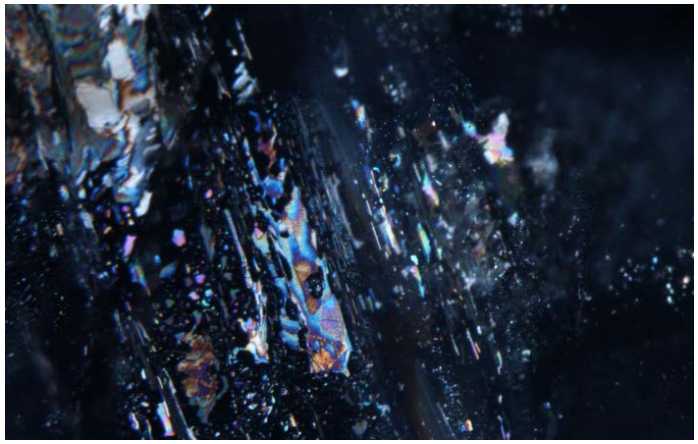

Figure 49: Iridescent naturally-healed fractures in GIA reference sample 100322689756. Darkfield and fiber-optic illumination. FOV 1.3 mm. Photo: C. Khowpong © GIA.

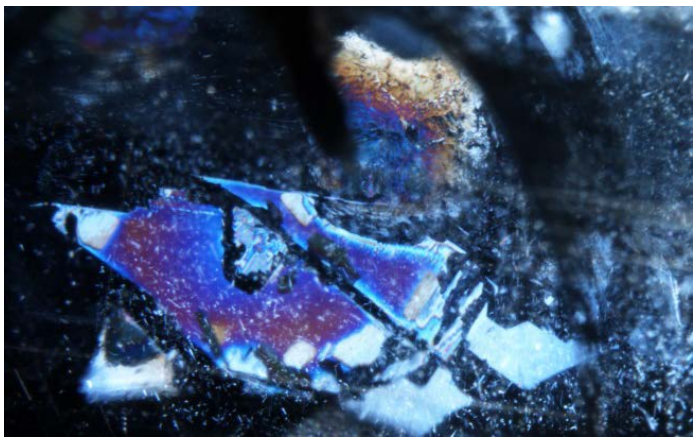

Figure 50: Naturally-healed fractures show up with interference colors in GIA reference sample 100322689760. Darkfield and fiber-optic illumination. FOV 2.7 mm. Photo: C. Khowpong © GIA.

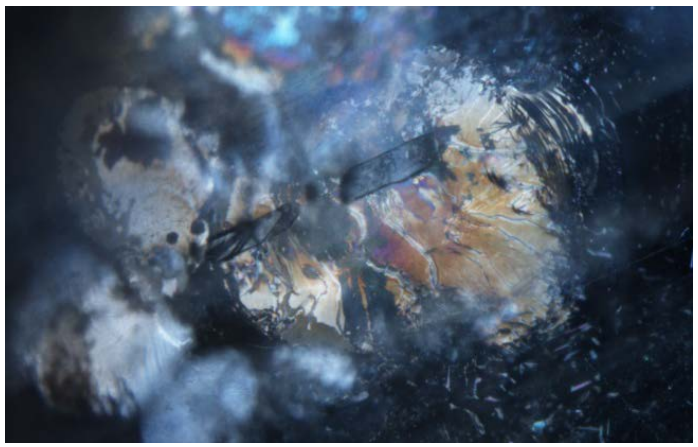

Figure 51: Negative crystals associated with iridescent naturally-healed fractures in GIA reference sample 100322689760. Darkfield and fiber-optic illumination. FOV 1.3 mm. Photo: C. Khowpong © GIA.

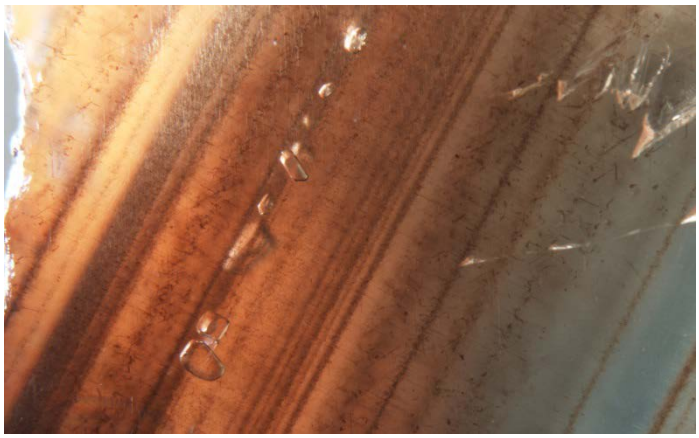

Figure 52: Trails of feldspar crystals (identified by Raman) along brownish needles in GIA reference sample 0669333402. Brightfield and diffused illumination. FOV 1.3 mm. Photo: C. Khowpong © GIA.

Figure 53: A plagioclase feldspar crystal surrounded by a naturally-healed fracture in GIA reference sample 100322689769. Brightfield and diffused illumination. FOV 2 mm. Photo: C. Khowpong © GIA.

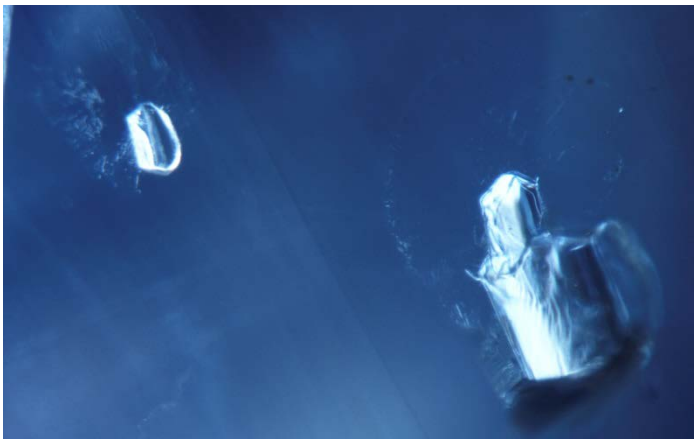

Figure 54: Two feldspar crystals with decrepitation discs in GIA reference sample 668889302. Darkfield and fiber-optic illumination. FOV 1.0 mm. Photo: V. Raynaud © GIA.

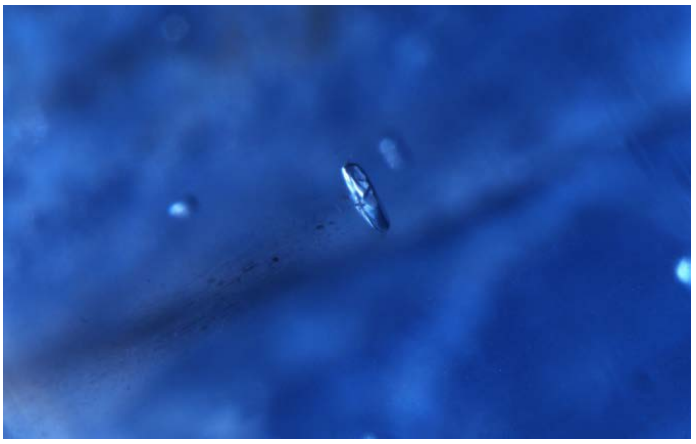

Figure 55: Elongated feldspar crystal with trail of particles in GIA reference sample 100322689774. Darkfield and fiber-optic illumination. FOV 1.3 mm. Photo: C. Khowpong © GIA.

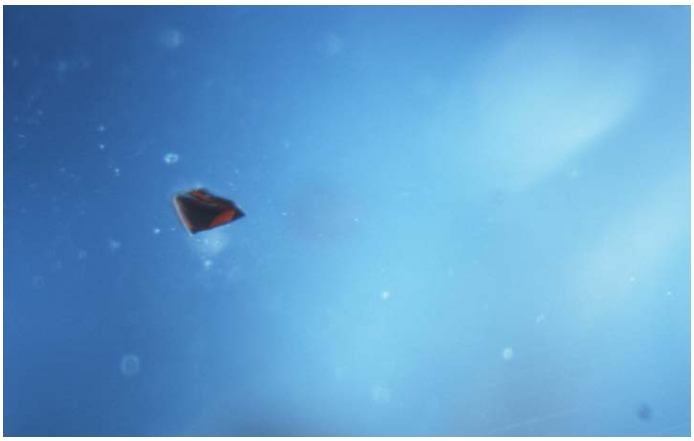

Figure 56: A brownish orangy crystal (identified by Raman as pyrochlore using the RRUFF database as a reference) in GIA reference sample 668889302. Darkfield and fiber-optic illumination. FOV 0.7 mm. Photo: V. Raynaud © GIA.

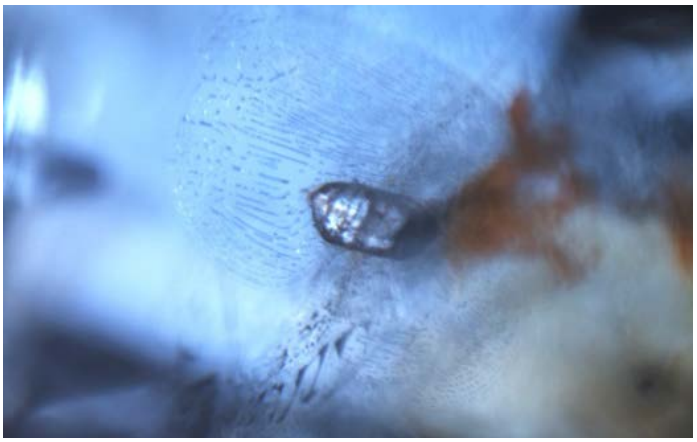

Figure 57: Zircon prism associated with tension halos in GIA reference sample 10030516118. Darkfield and fiber-optic illumination. FOV 1.2 mm. Photo: V. Raynaud © GIA.

Figure 58: Two crystals; zircon (front) and monazite (back) in GIA reference sample 100322689757. Darkfield and fiber-optic illumination. FOV 1.3 mm. Photo: C. Khowpong © GIA.

Figure 59: A bluish crystal (identified by Raman as molybdenite using the RRUFF database as a reference) in GIA reference sample 668889302. Darkfield and fiber-optic illumination. FOV 1.5 mm. Photo: V. Raynaud © GIA.

Figure 60: Negative crystal filled with goethite in GIA reference sample 100305161408. Darkfield and fiber-optic illumination. FOV 0.9 mm. Photo: S. Sangsawong © GIA.

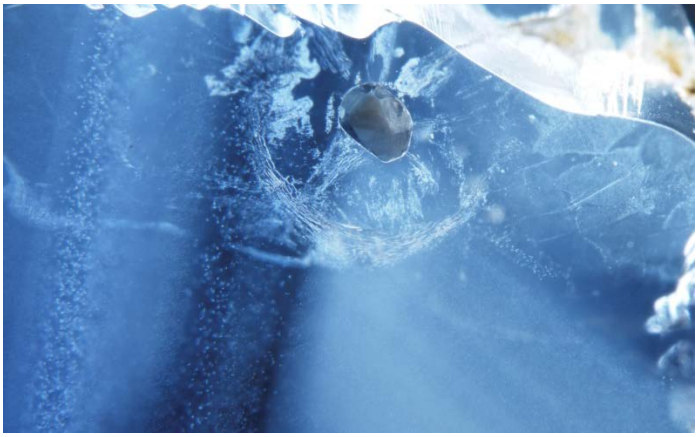

Figure 61: Unidentified crystal associated with naturally healed fractures in GIA reference sample 668841902. Darkfield and fiber-optic illumination. FOV 2.0 mm. Photo: V. Raynaud © GIA.

Figure 62: Mica associated with naturally-healed fractures in GIA reference sample 669333302. Darkfield illumination. FOV 0.8 mm. Photo: S. Sangsawong © GIA.

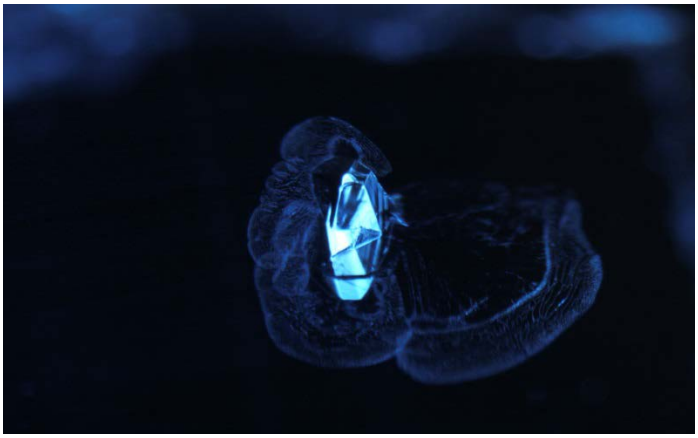

Figure 63: Negative crystal associated with a naturally-healed fracture in GIA reference sample 669301502. Darkfield illumination. FOV 3.6 mm. Photo: V. Raynaud © GIA.

## 3.2 Spectroscopy and chemistry of blue sapphires from Thailand

### 3.2.1 UV-VIS-NIR SPECTROSCOPY

UV-Vis-NIR spectra of blue/green Thai sapphire show features of $Fe^{3+}$ and $Fe^{2+}$-$Ti^{4+}$ as primary chromophores, which correspond to yellow and blue color, respectively. In addition, a strong absorption characteristic of basalt-related sapphires—around 840-800 nm in the near-infrared region—was present in all samples. The absorption features are identified as: (Ferguson, 1971, 1972; Hughes, 2017; chapter 4)

- An absorption shoulder at about 330 nm assigned to both $Fe^{3+}$ ions of an $Fe^{3+}$- $Fe^{3+}$ pairs. Its absorption strength increases more rapidly than the single $Fe^{3+}$ concentration (Figure 68).
- A peak at 377 and 450 nm assigned to $Fe^{3+}$- $Fe^{3+}$ pairs. These absorption peaks are distinctly and clearly due to high Fe content.
- A peak at 388 nm assigned to single $Fe^{3+}$ ions, therefore the absorption coefficient will increase linearly with $Fe^{3+}$ concentration.
- A band at about 535 nm assigned to $Fe^{3+}$- $Fe^{3+}$ pairs. It is only visible at high iron concentrations, such as in Thai yellow sapphire (Figure 64, yellow line).
- A band at about 700 nm of uncertain origin. However it seems to be visible when the iron concentration is high such as in Thai yellow sapphire (Figure 64, yellow line).
- A broad absorption band at 580 nm assigned to $Fe^{2+}$- $Ti^{4+}$ pairs, giving a blue color.
- And a broad absorption band around 840-880 nm at near infrared region which is characteristic of natural basalt-related blue sapphires. It is often attributed to $Fe^{2+}$- $Fe^{3+}$ pairs (Smith, 1977, 1978; Smith & Strens, 1976). Note that $Fe^{2+}$ in corundum is an acceptor; therefore it requires charge compensation by electron donors such as $Si^{4+}$or $Ti^{4+}$. This broad band is not clearly understood and requires further study. It could be due to charge compensation between $Fe^{2+}$ and $Ti^{4+}$, $Si^{4+}$ or both, as described in Hughes, 2017, chapter 4.

We selected three samples including GIA reference sample #4000, #5040, and #5039 to compare the UV-Vis-NIR spectra of blue/green Thai sapphire. Sample #7093 is also selected to represent yellow Thai sapphire for comparison. The absorption features are classified based on the sample colors as follows.

- *Blue dominant:* a strong absorption band of the $Fe^{2+}$-$Ti^{4+}$ chromophore at 580 nm is higher than absorption of $Fe^{3+}$ at 450nm. (Figure 65)
- *Yellow dominant:* an absorption band of $Fe^{3+}$ at 450 nm is higher than an absorption band of $Fe^{2+}$-$Ti^{4+}$ chromophore at 580 nm. (Figure 67)
- *Greenish dominant*: a mixture of the $Fe^{2+}$-$Ti^{4+}$ chromophore and $Fe^{3+}$. Usually E ray transmits more green light, whereas the O-ray transmits more blue. (Figure 70)

The features on these UV-Vis-NIR spectra are related to trace elements, as shown in Table 2. Sample #4000, #5039 and #5040 had Ti available to create blue color whereas sample #7093 had no Ti available which give yellow color. Sample #5039 and #5040 have similar Fe concentration, while sample #5039 has more Ti available than sample #5040; therefore sample #5039 has greenish blue color whereas sample #5040 has greenish yellow.

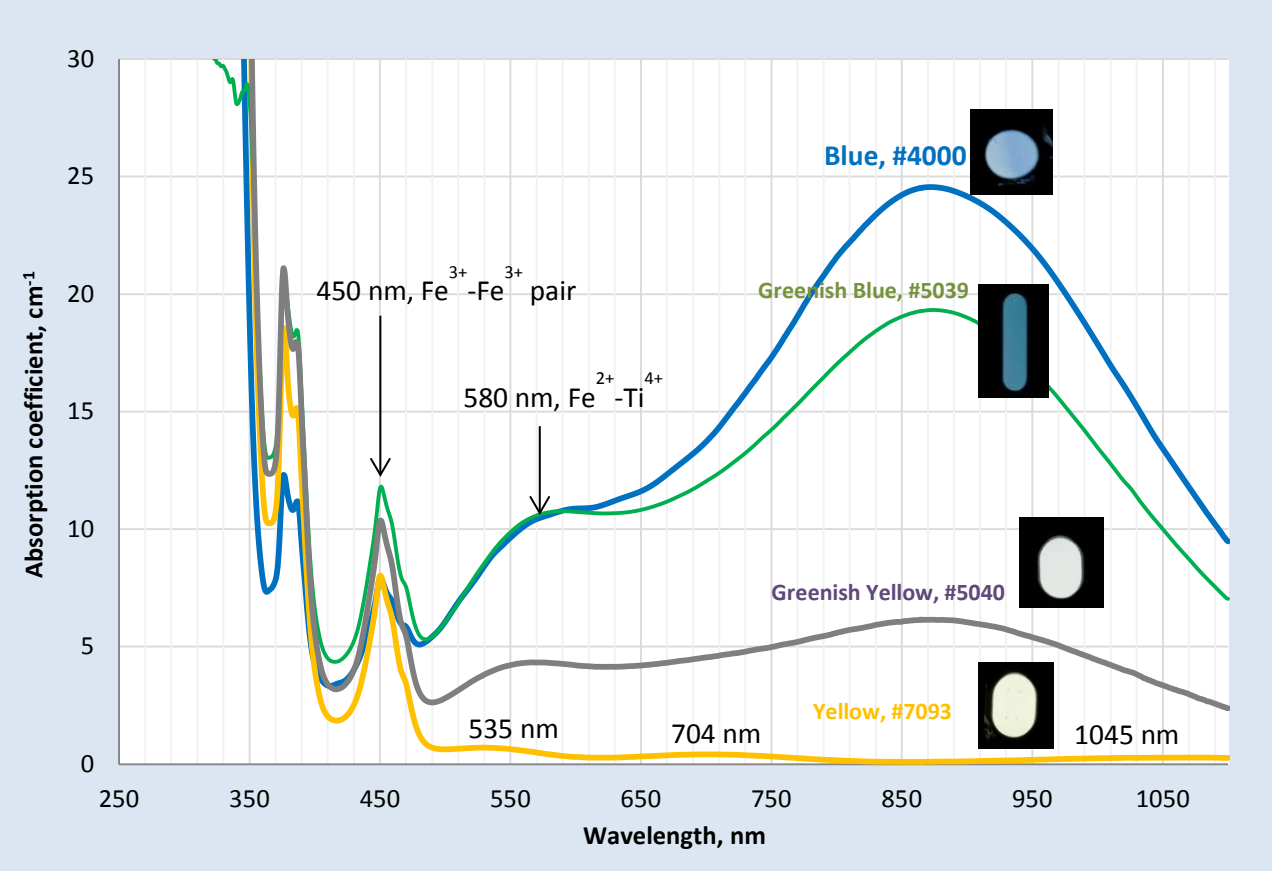


**Figure 64: Comparison O-ray spectra of blue/green/yellow Thai sapphire with inset color calibrated polarized photos of the beam path area for each sample. Optical path lengths are 1.065 mm for blue, 1.899 mm for greenish blue, 0.259 mm for greenish yellow, and 1.430 mm for yellow samples.**

**Table 2: LA-ICP-MS results in parts per million atomic (ppma) units for samples in Figure 63.**

| Color | $^{24}$Mg | $^{47}$Ti | [$^{47}$Ti] - [$^{24}$Mg] Or Ti available | $^{51}$V | $^{57}$Fe | $^{69}$Ga |
|---|---|---|---|---|---|---|
| Blue (#4000) | 4±0.8 | 17±4 | 13 | 1±0.1 | 2753±105 | 38±6 |
| Greenish blue (#5039) | 8±1 | 23±4 | 15 | 1±0.1 | 3738±174 | 39±1 |
| Greenish yellow (#5040) | 6±0.4 | 17±4 | 11 | 1±0.1 | 3898±253 | 37±6 |
| Yellow (#7093) | 14±0.4 | 9±1 | - | 0.5±0.1 | 3400±50 | 34±1 |

UV-Vis-NIR O- and E- ray spectra of samples #4000, #5039, #5040, are presented below along with chemistry data collected in the same area.

### *Blue Sapphire from GIA reference sample #4000*

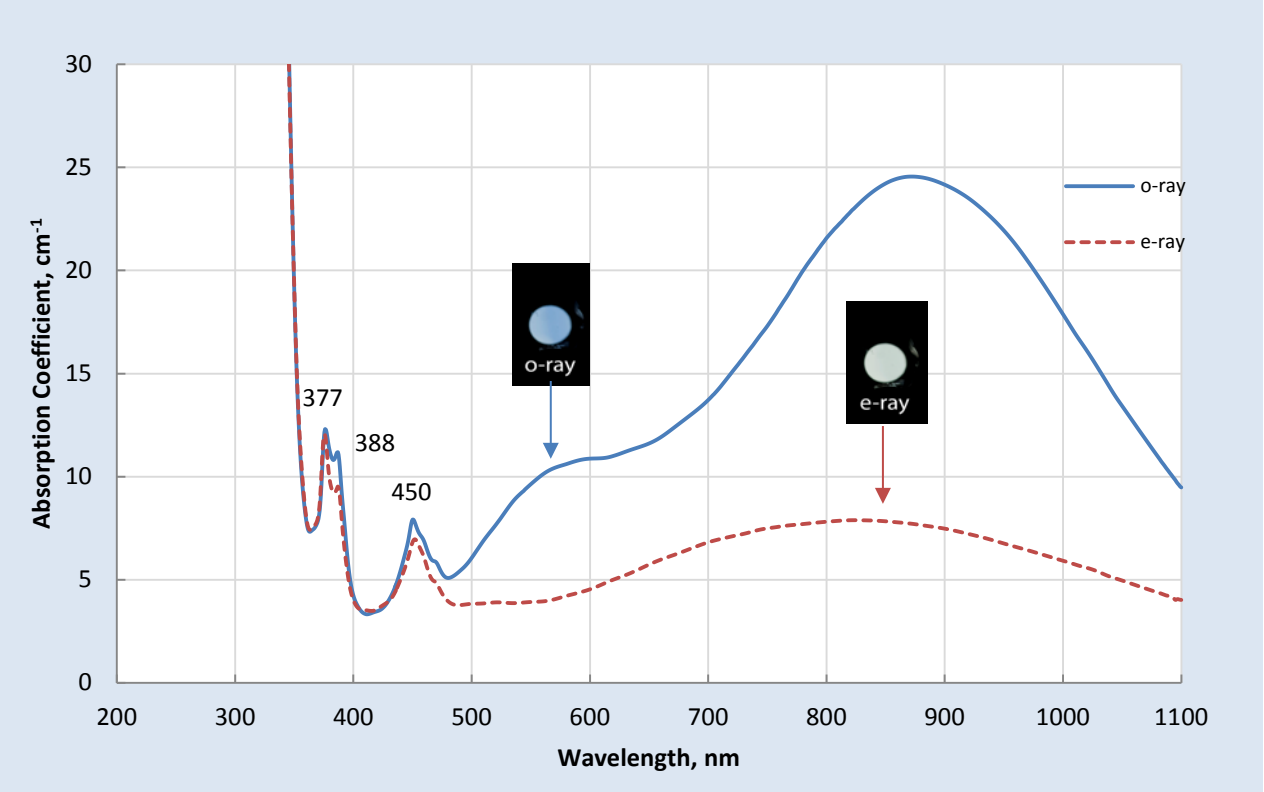


Figure 65: Polarized UV-Vis-NIR absorption spectra of GIA reference specimen #4000 with inset color calibrated polarized photos of the beam path area for the o- and e-rays. Optical path length: 1.065 mm. Weight: 0.234 carats. Color: blue.

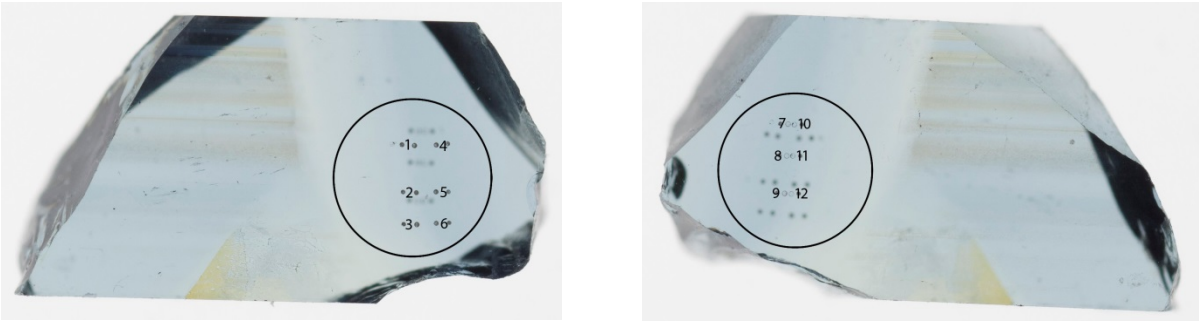

Figure 66: GIA reference sample #4000 showing the location of the 12 spots where LA-ICP-MS analysis was conducted on each side of the wafer. Field of view 6.00 mm. Photo: S. Engniwat © GIA.

**Table 3: LA-ICP-MS results in parts per million atomic (ppma) units for GIA reference sample #40002. "BDL" stands for "Below Detection Limit", "BQL" stands for "Below Quantification Limit"**

| GIA Ref Sample #4000 (color of the area) | $^{9}$Be | $^{24}$Mg | $^{47}$Ti | $^{51}$V | $^{52}$Cr | $^{57}$Fe | $^{69}$Ga | $^{90}$Zr | $^{93}$Nb | $^{178}$Hf | $^{181}$Ta | $^{182}$W | $^{232}$Th |
|---|---|---|---|---|---|---|---|---|---|---|---|---|---|
| SP1 (blue) | BDL | 4 | 19 | 1 | BQL | 2614 | 35 | BDL | BDL | BDL | BDL | BDL | BDL |
| SP2 (blue) | BDL | 5 | 22 | 1 | BQL | 2800 | 37 | BDL | BQL | BDL | BDL | BDL | BDL |
| SP3 (blue) | BDL | 6 | 21 | 1 | BQL | 2939 | 38 | BDL | BDL | BQL | BDL | BDL | BDL |
| SP4 (blue) | BDL | 4 | 17 | 1 | BQL | 2647 | 34 | BDL | BDL | BDL | BDL | BDL | BQL |
| SP5 (blue) | BDL | 5 | 19 | 1 | BQL | 2658 | 35 | BDL | BDL | BQL | BDL | BDL | BDL |
| SP6 (blue) | BDL | 5 | 18 | 1 | BQL | 2760 | 35 | BQL | BDL | BDL | BDL | BDL | BDL |
| SP7 (blue) | BDL | 4 | 20 | 1 | 2 | 2716 | 37 | BDL | BDL | BQL | BDL | BDL | BDL |
| SP8 (blue) | BDL | 4 | 18 | 1 | 2 | 2782 | 57 | BDL | BQL | BDL | BQL | BDL | BDL |
| SP9 (blue) | BQL | 3 | 9 | 1 | 2 | 2779 | 37 | BDL | BQL | 0.000 | 0.001 | 0.085 | BDL |
| SP10 (blue) | 0.21 | 4 | 18 | 1 | 2 | 2706 | 36 | BDL | BDL | BQL | BDL | BDL | BQL |
| SP11 (blue) | BDL | 4 | 11 | 1 | 3 | 2695 | 35 | BDL | BDL | BDL | BQL | BDL | BDL |
| SP12 (blue) | BDL | 4 | 11 | 1 | 2 | 2943 | 36 | BDL | BQL | BDL | BQL | BDL | BDL |
| **Average±SD** | **-** | **4±0.8** | **17±4** | **1±0.1** | **-** | **2753±105** | **38±6** | **-** | **-** | **-** | **-** | **-** | **-** |
| ***Detection limit*** | ***0.06*** | ***0.1*** | ***0.3*** | ***0.03*** | ***0.4*** | ***1*** | ***0.01*** | ***0.001*** | ***0.001*** | ***0.000*** | ***0.000*** | ***0.001*** | ***0.000*** |

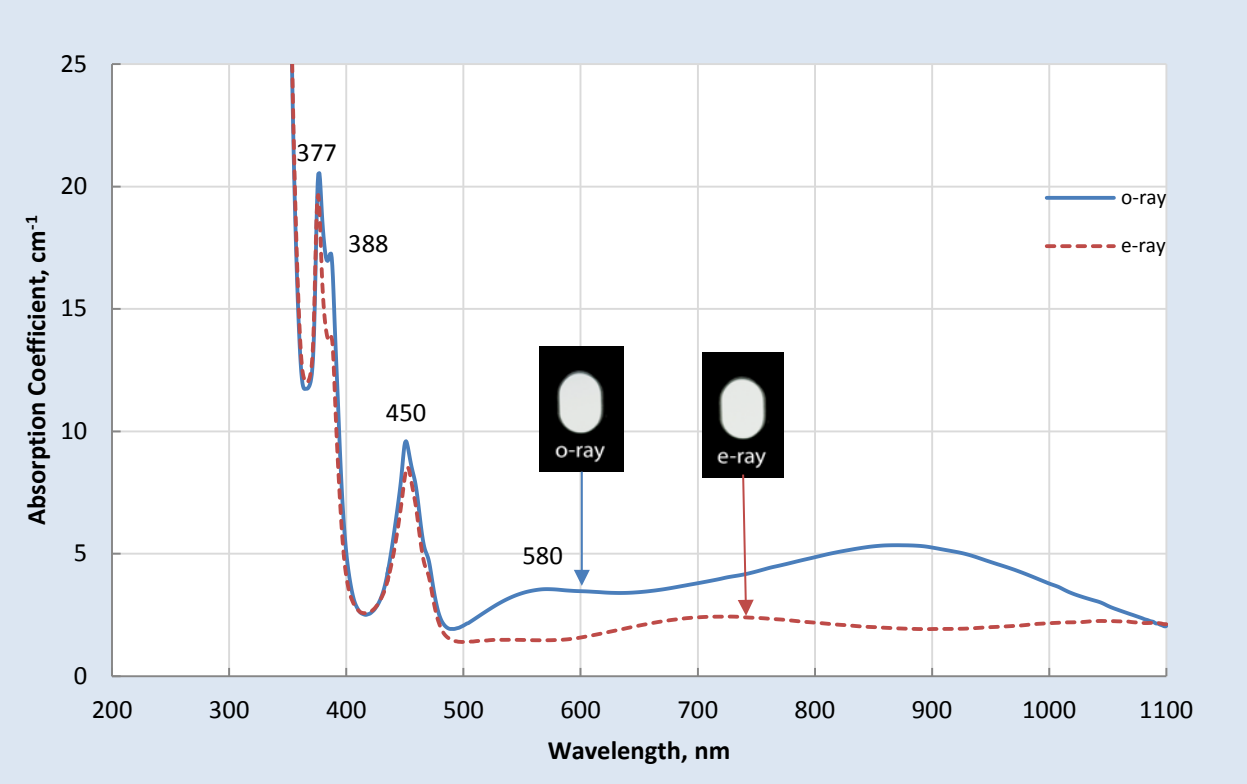


Figure 67: Polarized UV-Vis-NIR absorption spectra of GIA reference specimen #5040 with inset color calibrated polarized photos of the beam path area for the o- and e-rays. Optical path length: 0.259 mm. Weight: 0.058 carats. Color: greenish yellow.

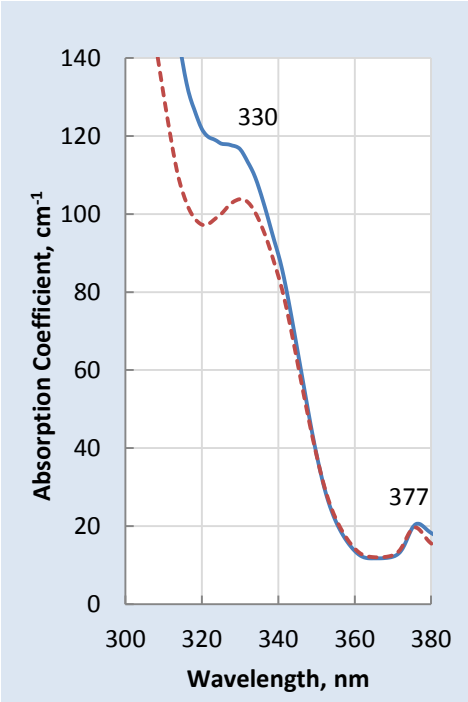


Figure 68: Expanded polarized UV-Vis-NIR absorption spectra of GIA reference specimen #5040 showing the 330 nm absorption band.


**Figure 69: GIA reference sample #5040 showing the location of the 12 spots where LA-ICP-MS analysis was conducted on each side of the wafer. Field of view 3.00 mm. Photo: S. Engniwat © GIA.**

**Table 4: LA-ICP-MS results in parts per million atomic (ppma) units for GIA reference sample #5040.**

| GIA Ref Sample #5040 (color of the area) | 9Be | 24Mg | 47Ti | 51V | 52Cr | 57Fe | 69Ga | 90Zr | 93Nb | 178Hf | 181Ta | 182W | 232Th |
|---|---|---|---|---|---|---|---|---|---|---|---|---|---|
| SP1 (yellowish green) | BDL | 6 | 15 | 1 | BDL | 3834 | 38 | BDL | BDL | BQL | BDL | BDL | 0 |
| SP2 (yellowish green) | BDL | 6 | 12 | 1 | BDL | 3761 | 36 | BQL | BQL | BDL | BDL | BQL | BDL |
| SP3 (yellowish green) | 0 | 6 | 10 | 0 | BQL | 3797 | 36 | BDL | BDL | BDL | BDL | 0.038 | BDL |
| SP4 (yellowish green) | BDL | 6 | 14 | 1 | BDL | 3724 | 37 | BDL | BDL | BDL | BDL | BDL | BDL |
| SP5 (yellowish green) | BDL | 6 | 13 | 0 | BDL | 3943 | 38 | BDL | BDL | BDL | BQL | BDL | BDL |
| SP6 (yellowish green) | BDL | 6 | 11 | 1 | BDL | 3761 | 37 | BDL | BDL | BDL | 0.003 | BDL | BDL |
| SP7 (yellowish green) | BDL | 6 | 9 | 1 | BQL | 3907 | 38 | BDL | BQL | BDL | 0.001 | BDL | BDL |
| SP8 (yellowish green) | BQL | 6 | 9 | 1 | BQL | 3870 | 37 | BDL | BDL | BDL | 0.001 | BDL | BQL |
| SP9 (yellowish green) | BQL | 5 | 11 | 1 | 2 | 3797 | 37 | BDL | BDL | BDL | 0.001 | BDL | BQL |
| SP10 (yellowish green) | BQL | 6 | 9 | 1 | 1 | 4674 | 39 | BDL | BQL | BDL | 0.001 | BDL | BDL |
| SP11 (yellowish green) | BDL | 6 | 9 | 1 | BQL | 3870 | 39 | BDL | BDL | BDL | 0.001 | BDL | BDL |
| SP12 (yellowish green) | BDL | 5 | 10 | 1 | 1 | 3834 | 37 | BDL | BDL | BDL | 0.001 | BDL | BDL |
| **Average±SD** | - | **6±0.4** | **17±4** | **1±0.1** | - | **3898±253** | **37±6** | - | - | - | **0.01±0.01** | - | - |
| ***Detection limit*** | ***0.06*** | ***0.1*** | ***0.3*** | ***0.03*** | ***0.4*** | ***1*** | ***0.02*** | ***0.001*** | ***0.001*** | ***0.001*** | ***0.000*** | ***0.001*** | ***0.000*** |

### *Greenish Blue from GIA reference sample #5039*

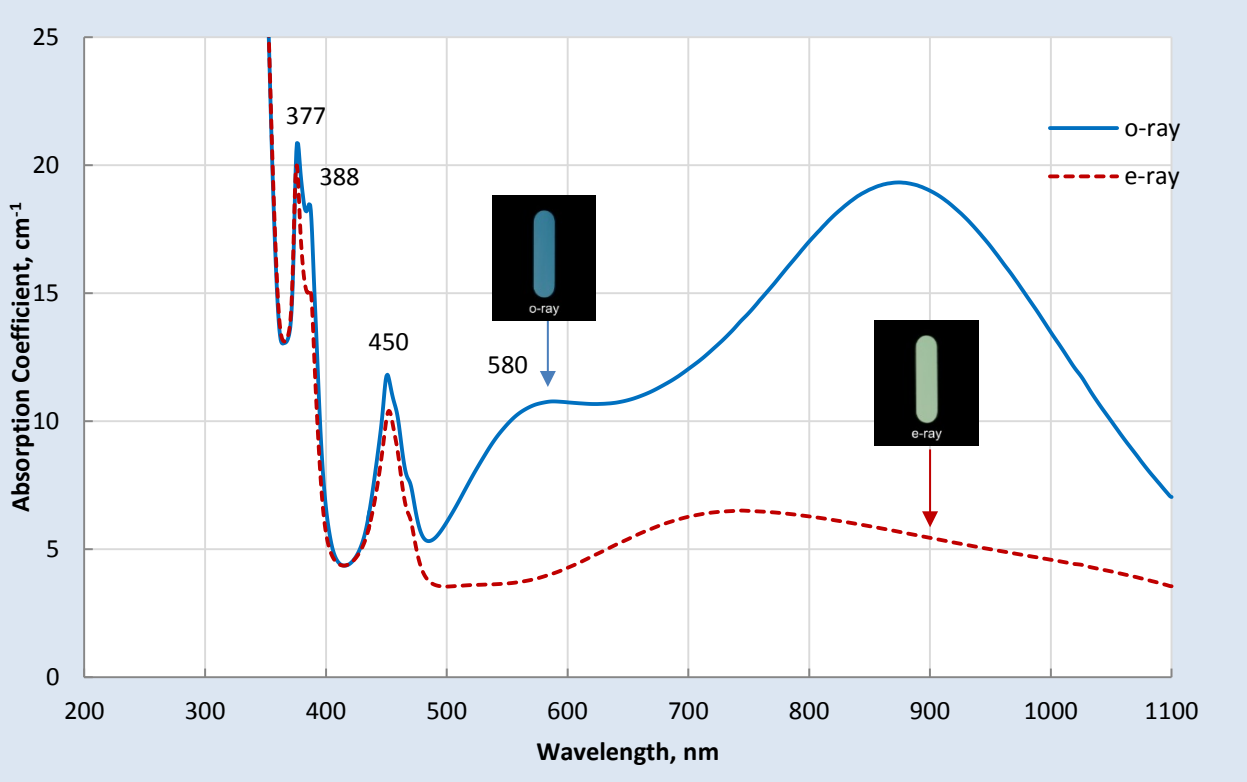


**Figure 70: Polarized UV-Vis-NIR absorption spectra of GIA reference specimen #5039 with inset color calibrated polarized photos of the beam path area for the o- and e-rays. Optical path length: 1.899 mm. Weight: 1.046 carats. Color: greenish blue**

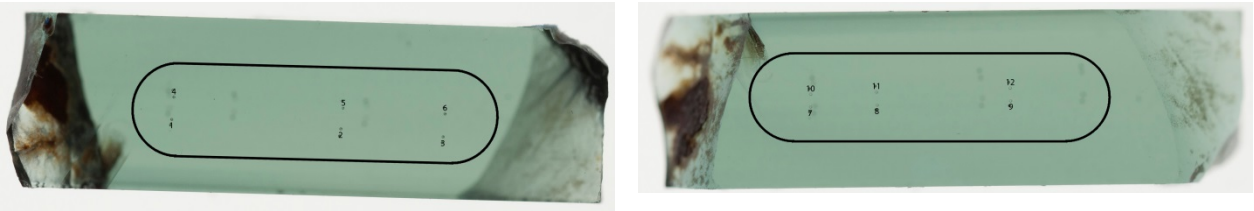

**Figure 71: GIA reference sample #5039 showing the location of the 12 spots where LA-ICP-MS analysis was conducted on each side of the wafer. Field of view 3.00 mm. Photo: S. Engniwat © GIA.**

Table 5: LA-ICP-MS results in parts per million atomic (ppma) units for GIA reference sample #5039.

| GIA Ref Sample #5039 (color of the area) | 9Be | 24Mg | 47Ti | 51V | 52Cr | 57Fe | 69Ga | 90Zr | 93Nb | 178Hf | 181Ta | 182W | 232Th |
|---|---|---|---|---|---|---|---|---|---|---|---|---|---|
| SP1 (greenish blue) | BDL | 8 | 20 | 1 | BDL | 3980 | 39 | BDL | BDL | BDL | BQL | BDL | BDL |
| SP2 (greenish blue) | BDL | 8 | 25 | 1 | BQL | 3980 | 40 | BDL | BQL | BDL | BQL | BDL | BDL |
| SP3 (greenish blue) | BDL | 7 | 20 | 1 | BQL | 4016 | 39 | BDL | BQL | BDL | 0.001 | BDL | BDL |
| SP4(greenish blue) | BDL | 7 | 15 | 1 | BDL | 3688 | 37 | BDL | BDL | BDL | BQL | BDL | 0.002 |
| SP5 (greenish blue) | BDL | 7 | 17 | 1 | BQL | 3651 | 39 | BDL | BDL | BDL | BDL | BDL | BDL |
| SP6 (greenish blue) | BQL | 7 | 24 | 1 | BQL | 3870 | 37 | BQL | BQL | BDL | 0.001 | BDL | BDL |
| SP7 (greenish blue) | BDL | 8 | 26 | 1 | BDL | 3633 | 40 | BDL | BDL | BDL | BQL | BDL | BDL |
| SP8 (greenish blue) | BDL | 9 | 25 | 1 | BQL | 3637 | 41 | 0.004 | BDL | BQL | BQL | BDL | BDL |
| SP9 (greenish blue) | BDL | 8 | 27 | 1 | BDL | 3505 | 40 | BQL | BDL | BDL | 0.001 | BDL | BDL |
| SP10 (greenish blue) | BQL | 8 | 26 | 1 | BQL | 3629 | 40 | BDL | BDL | BDL | BDL | BDL | BQL |
| SP11 (greenish blue) | BQL | 9 | 25 | 1 | BDL | 3688 | 41 | BQL | BDL | BQL | BQL | BDL | BDL |
| SP12 (greenish blue) | BDL | 8 | 24 | 1 | BDL | 3589 | 39 | BQL | BDL | BDL | BQL | BDL | BDL |
| **Average±SD** | - | **8±1** | **23±4** | - | - | **3738±174** | **39±1** | - | - | - | - | - | - |
| ***Detection limit*** | ***0.1*** | ***0.3*** | ***3*** | ***0.3*** | ***0.7*** | ***1*** | ***0.1*** | ***0.01*** | ***0.02*** | ***0.001*** | ***0.001*** | ***0.001*** | ***0.001*** |

### 3.2.2 FOURIER TRANSFORM INFRARED SPECTROSCOPY OR FTIR

Five (5) samples were selected to represent FTIR spectra in Thai sapphires. FTIR spectra were collected through the same areas where UV-Vi-NIR spectra for GIA reference sample #4000, #5040, and #5039 were taken, see Figure 72(a-c). Samples #4000 and #5039 presented a single peak at 3309 $cm^{-1}$ which is the most frequently found in Thai sapphire, whereas sample #5040 revealed no diagnostic features. Blue sapphire #5470 showed strong 3309 $cm^{-1}$ peak together with features at 3368 and 3232 $cm^{-1}$, which are related to the OH stretching mode of water in corundum (Hughes, 2017, chapter 4). Features attributed to minerals such as kaolinite are also often observed in Thai sapphire.

Figure 72: Un-oriented FTIR spectra of GIA reference sample #4000, #5040, #5039, #4702 and #9769 in the 2800 to 3600 $cm^{-1}$ range. Optical path length: a) 0.166; b) 0.234, c) 0.058 and d) 3.49 mm.
* Without the polarizer in the FTIR spectrometer, it wasn't possible to obtain accurate optical FTIR spectra.

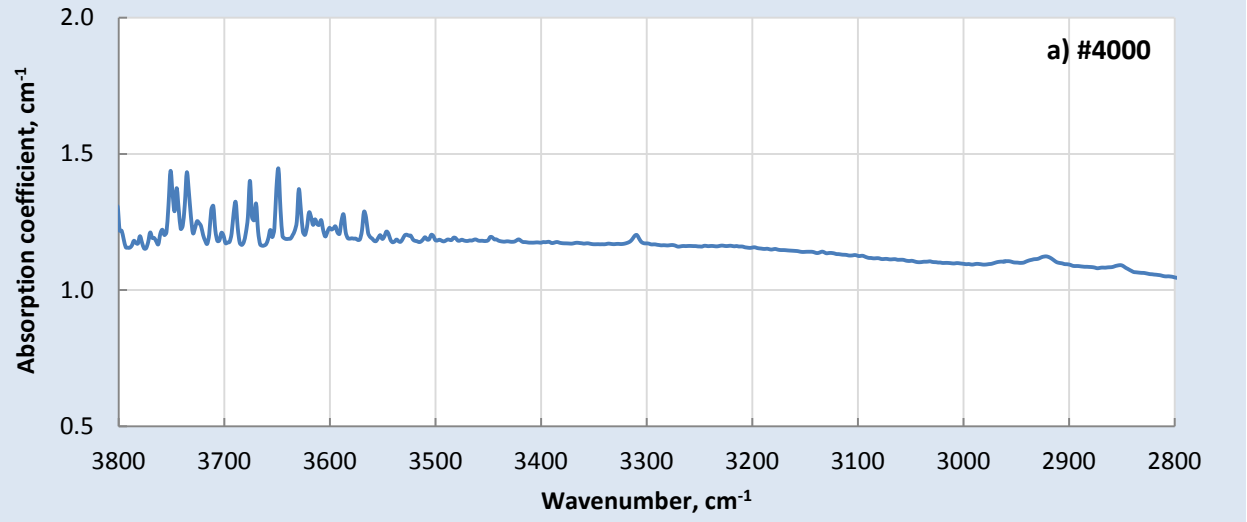


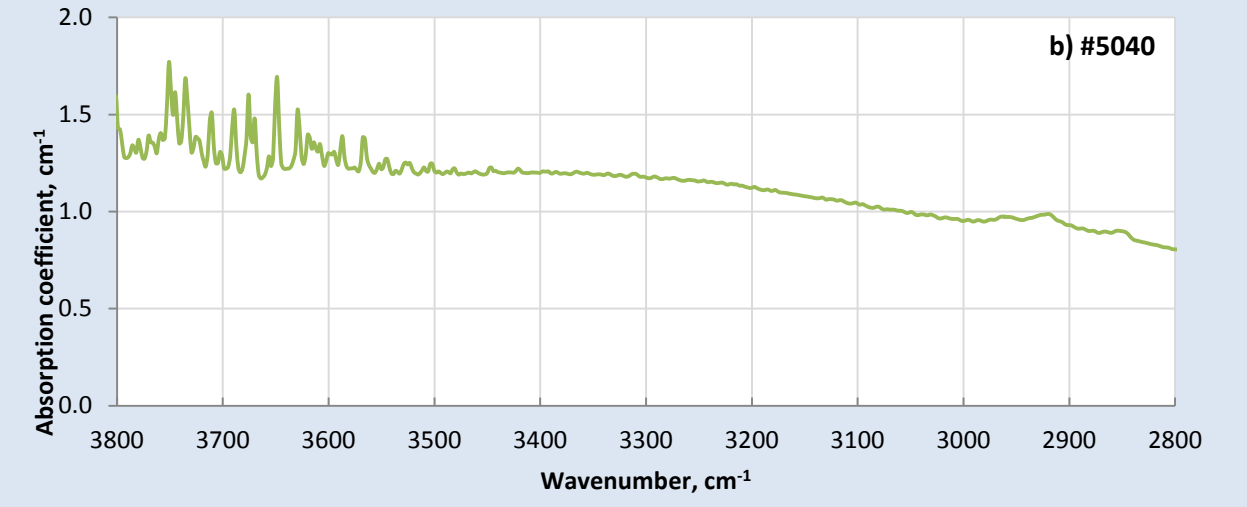


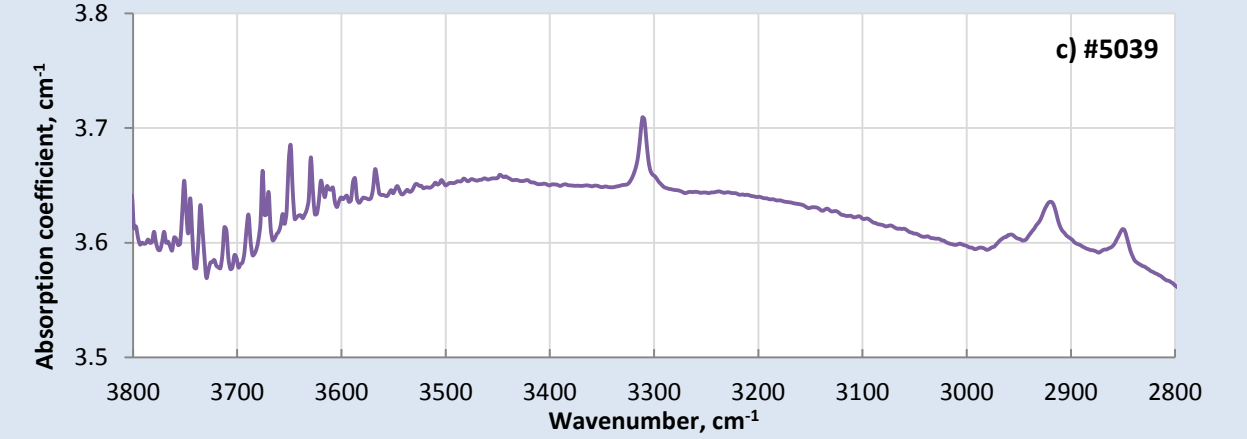

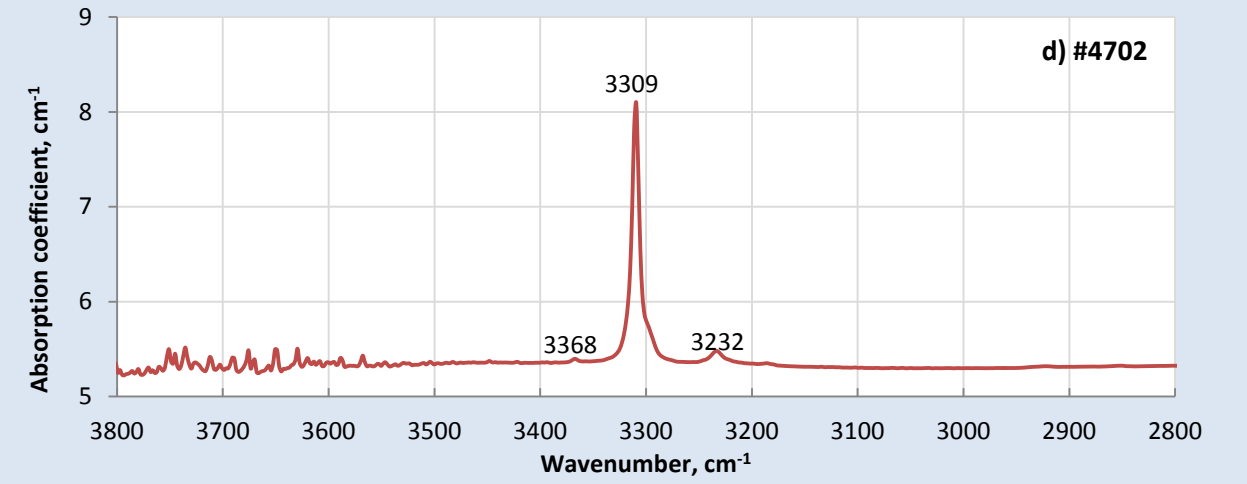


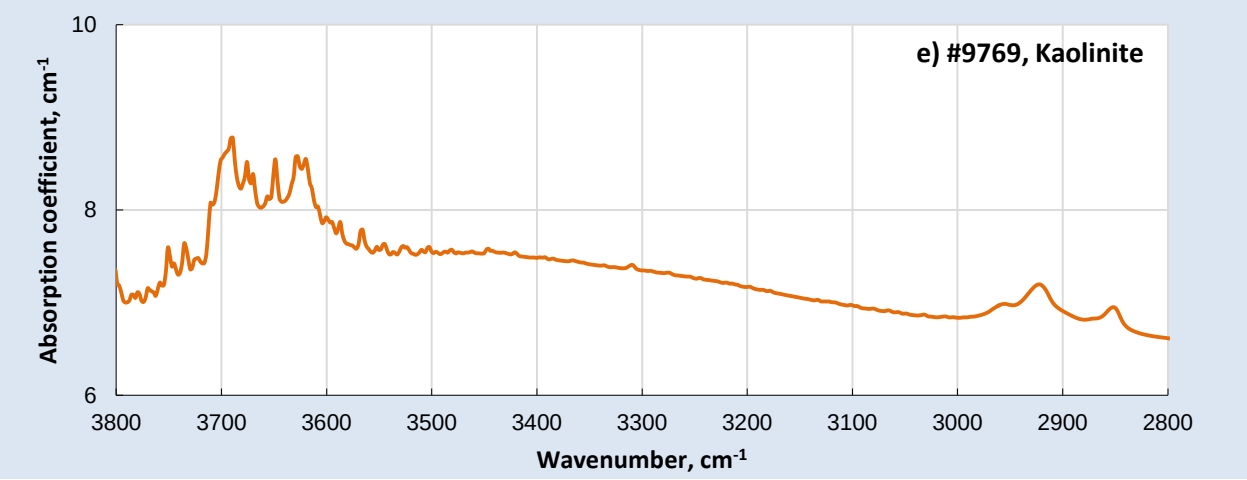


### 3.2.3 CHEMICAL ANALYSIS

The trace element chemistry of Sixty (60) Thai sapphire samples was analyzed using LA-ICP-MS. All samples contained significant amounts of Fe and traces of Mg, Ti, and Ga, which are normal elements found in sapphire. The Mg concentrations in basalt-related sapphires are lower than metamorphic sapphires. For example, sapphires from Baw Mar, Myanmar had Mg concentrations up to 102 ppma. (Soonthorntantikul, 2017). Fe concentration varies strongly, from 675 to 2987 ppma in blue sapphire samples and from 1884 to 4966 ppma for greenish blue sapphires. Blue sapphires contained up to 23 ppma vanadium (V) and a maximum of 35 ppma chromium (Cr), whereas greenish sapphire often presented lower concentrations of both elements as shown in Table6.

Areas with brown particle inclusions showed higher concentrations of Mg, Ti, and Fe than areas without these inclusions. Some heavy elements—mainly tantalum (Ta)—were commonly detected as shown in GIA reference sample #9802 and #3402.

Table 6: LA-ICP-MS results in parts per million atomic (ppma) in blue and greenish-blue sapphire from Chantaburi, Thailand

| Min-max (average±SD) | $^{24}$Mg | $^{47}$Ti | $^{51}$V | $^{53}$Cr | $^{57}$Fe | $^{69}$Ga |
|---|---|---|---|---|---|---|
| Blue (Figure 15, top); n=28 | 2-19 (7±3) | 9-95 (41±28) | 1-23 (8±5) | 1-35 (5±5) | 675-2987 (1723±669) | 33-57 (39±4) |
| Greenish blue (Figure 15, bottom); n=31 | 3+50 (9±6) | 5-91 (23±13) | 0-6 (1±1) | 1-11 (4±2) | 2406-4966 (3672±527) | 27-54 (37±3) |

## *GIA reference sample #9802*

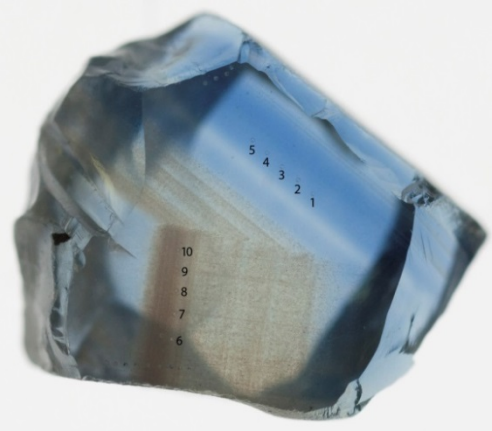


We analyzed chemistry in blue areas and areas dominated by brown needles or particles. $Mg^{2+}$ is charge compensated with $Ti^{4+}$ and the concentration of $Ti^{4+}$ is high enough to leave available ions to pair with $Fe^{2+}$, creating the blue color. In areas with brown needles, Mg, Ti, and Fe showed higher concentrations than in blue areas. This is related to the presence of inclusions of hematite ($Fe_2O_3$) and rutile ($TiO_2$) confirmed by Raman spectrometry. No significant heavy elements were detected.

Figure 73: GIA reference sample #9802 showing the location of the 12 spots where LA-ICP-MS analysis was conducted on the wafer. Field of view 6.00 mm. Photo: S. Engniwat © GIA.

Table 7: LA-ICP-MS results in parts per million atomic (ppma) units for GIA reference sample #9802.

| Laser spot number (colour of the area) | $^{9}$Be | $^{24}$Mg | $^{47}$Ti | $^{51}$V | $^{52}$Cr | $^{56}$Fe | $^{69}$Ga | $^{90}$Zr | $^{93}$Nb | $^{178}$Hf | $^{181}$Ta | $^{182}$W | $^{232}$Th |
|---|---|---|---|---|---|---|---|---|---|---|---|---|---|
| SP1 (blue) | BDL | 7 | 17 | 5 | 2 | 1921 | 35 | 0.003 | BDL | BDL | BDL | BDL | BDL |
| SP2 (blue) | BDL | 6 | 14 | 5 | 3 | 1986 | 35 | BDL | BDL | BDL | BDL | BDL | BQL |
| SP3 (blue) | BDL | 7 | 16 | 6 | 3 | 1972 | 36 | BDL | BDL | BDL | BDL | BQL | BDL |
| SP4 (blue) | BDL | 7 | 14 | 4 | 2 | 1884 | 34 | BDL | 0.02 | BDL | BQL | BQL | BDL |
| SP5(blue) | BDL | 7 | 16 | 5 | 2 | 1950 | 34 | BDL | BDL | BDL | BDL | BDL | BQL |
| **Average±SD** | | **7±0.2** | **15±1.4** | **5±0.4** | **2±0.5** | **1942±41** | **35±0.7** | | | | | | |
| sp 6 (brown needles) | BDL | 9 | 42 | 6 | BQL | 2151 | 37 | BQL | BDL | BDL | BDL | BDL | BDL |
| sp 7 (brown needles) | BDL | 8 | 54 | 6 | 2 | 2114 | 36 | BDL | BDL | BDL | BDL | BDL | BDL |
| sp 8 (brown needles) | BDL | 8 | 46 | 6 | BQL | 2118 | 36 | BDL | BDL | BDL | BDL | BDL | BQL |
| sp 9 (brown needles) | BQL | 9 | 54 | 6 | BQL | 2078 | 36 | BDL | BQL | BDL | BQL | BDL | BDL |
| sp 10 (brown needles) | BDL | 8 | 44 | 6 | BQL | 2030 | 35 | BQL | BDL | BDL | BDL | BDL | BDL |
| **Average±SD** | | **8±0.3** | **48±5.7** | **6±0.1** | | **2098±46** | **36±0.8** | | | | | | |
| ***Detection Limit (ppma)*** | ***0.3*** | ***0.4*** | ***0.8*** | ***0.05*** | ***0.5*** | ***3*** | ***0.02*** | ***0.001*** | ***0.001*** | ***0.000*** | ***0.000*** | ***0.001*** | ***0.001*** |

### *GIA reference sample #3402*

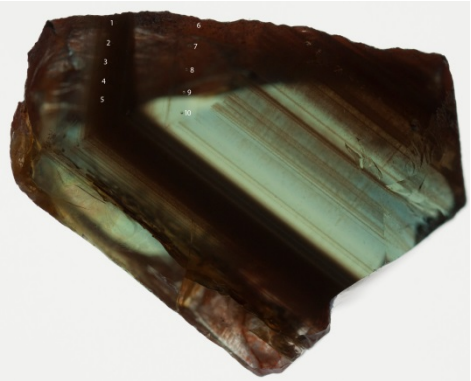

**Figure 74: GIA reference sample 669333402 showing the location of the 18 spots where LA-ICP-MS analysis was conducted on the wafer. Field of view 8.00 mm. Photo: S. Engniwat © GIA.**

This sample is representative for greenish blue sapphires that contain brown needles. We analyzed chemistry on non-included areas and areas with brown needles. In comparison with #9802, this sample contained higher amounts of Fe, which caused a yellow color component to give greenish blue when combined with blue. Chemistry in included areas showed higher Mg, Ti, and Fe content than in non-included areas, which is similar to sample #9802. In addition, Mn was detected at about 0.5 ppma in areas with brown needles. This could be related to another mineral. Chemistry suggests brown needles are hematite ($Fe_2O_3$) and rutile ($TiO_2$) characterized the brown needles by Raman spectroscopy. The results matched with hematite ($Fe_2O_3$) and rutile ($TiO_2$) (Figure 75). All spectra were compared with the RRUFF reference database.

**Table 8: LA-ICP-MS results in parts per million atomic (ppma) units for GIA reference sample #3402.**

| Laser spot number (colour of the area) | $^{9}$Be | $^{24}$Mg | $^{47}$Ti | $^{51}$V | $^{52}$Cr | $^{56}$Fe | $^{69}$Ga | $^{90}$Zr | $^{93}$Nb | $^{178}$Hf | $^{181}$Ta | $^{182}$W | $^{232}$Th |
|---|---|---|---|---|---|---|---|---|---|---|---|---|---|
| sp 1 (pale blue) | BDL | 8 | 12 | 0.89 | 8 | 3724 | 35 | BDL | BDL | BDL | BDL | BDL | BDL |
| sp 2 (pale blue) | BDL | 8 | 10 | 0.79 | 7 | 3870 | 35 | BQL | BDL | BDL | BQL | BQL | BDL |
| sp 3 (pale blue) | BDL | 7 | 11 | 0.80 | 11 | 3761 | 35 | BDL | BDL | BDL | BDL | BDL | BDL |
| sp 4 (pale blue) | BDL | 8 | 13 | 0.78 | 9 | 3834 | 35 | BDL | BDL | BDL | BQL | BDL | BDL |
| sp 5 (pale blue) | BDL | 8 | 13 | 0.67 | 6 | 3724 | 35 | BDL | BDL | BDL | BDL | BDL | BDL |
| **Average±SD** | | **8±0.4** | **12±1** | **0.8±0.1** | **8±2** | **3783±66** | **35±0.3** | | | | | | |
| sp 6 (brown needles) | BDL | 12 | 41 | 0.68 | BDL | 4966 | 43 | BQL | BDL | BDL | 0.01 | BDL | BDL |
| sp 7 (brown needles) | BDL | 11 | 44 | 0.58 | BQL | 4491 | 37 | 0.00 | BQL | BDL | 0.02 | BDL | BDL |
| sp 8 (brown needles) | BDL | 11 | 45 | 0.71 | BQL | 4418 | 37 | 0.00 | BDL | BDL | 0.01 | BDL | BQL |
| sp 9 (brown needles) | BDL | 11 | 40 | 0.68 | BDL | 4418 | 38 | BQL | BDL | BDL | 0.01 | BQL | BDL |
| sp 10 (brown needles) | BDL | 10 | 46 | 0.56 | BQL | 4491 | 37 | BQL | BDL | 0.00 | 0.01 | BDL | BDL |
| **Average±SD** | | **11±1** | **43±3** | **1±0.1** | | **4557±231** | **38±3** | | | | | | |
| ***Detection Limit (ppma)*** | **0.3** | **0.4** | **0.8** | **0.05** | **0.5** | **3** | **0.02** | **0.001** | **0.001** | **0.000** | **0.000** | **0.001** | **0.001** |

Figure 75: Raman spectrum of GIA reference sample #3402 obtained from an area with brownish particles was compared with known spectra from the RRUFF database and identified as a mixture of corundum, hematite, and rutile. Note: Rt=rutile, Hem=hematite, and Crn=corundum.

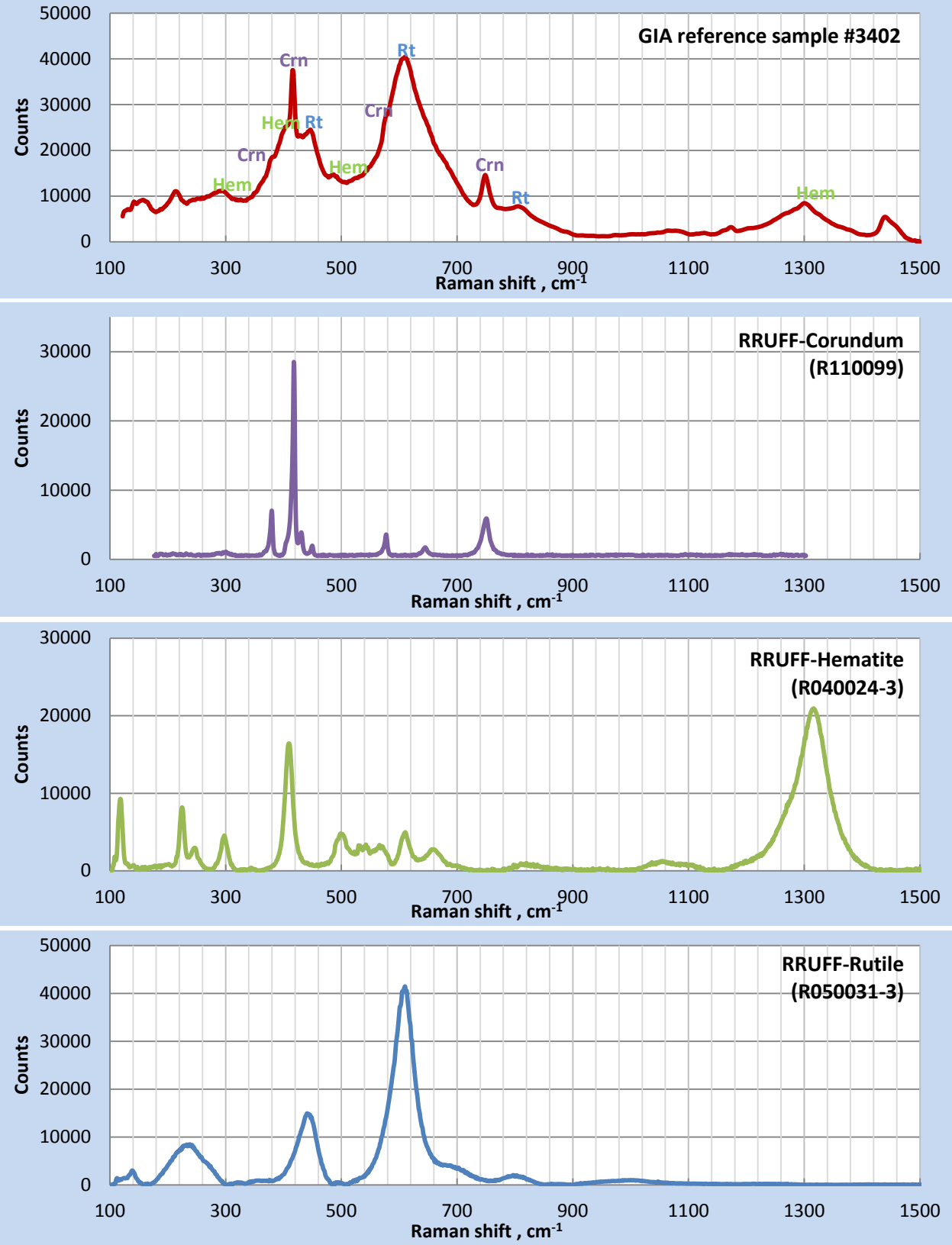

## 3.3 Comparison between Thai blue sapphire and other basalt-related sapphires

Blue sapphires related to alkali basalts, are common in the marketplace. The most known sources are Australia, Thailand, Cambodia and Nigeria. Since sapphires from these sources have a very similar origin, it is very challenging to discriminate between these sources.

We compared FTIR results from Thai blue sapphires with other basalt-related sapphires that have not been treated. Cambodia and Nigeria commonly found 3309 series whereas Australia and Thailand detected 3309 $cm^{-1}$ with 3368 and 3232, and 3186 $cm^{-1}$ only. The majority of Thai sapphires showed single 3309 $cm^{-1}$ or 27 (out of 46) samples in this study. Moreover we found 6 samples with no diagnostic feature. Peaks related to the presence of kaolinite are detected in all basalt related sapphires.

**Table 9: Comparison of FTIR features in basalt-related sapphires from different localities. Note: 3309 series including 3394, 3379, 3368, 3309, 3232, and 3186 $cm^{-1}$.**

| Country | Total sample number | Frequency found (%) | | | | | | Mineral (Kaolinite) |
|---|---|---|---|---|---|---|---|---|
| | | 3394 $cm^{-1}$ | 3379 $cm^{-1}$ | 3368 $cm^{-1}$ | 3309 $cm^{-1}$ | 3232 $cm^{-1}$ | 3186 $cm^{-1}$ | |
| **Australia** | 42 | | | 66.7 | 100 | 83.3 | 50.0 | 35.7 |
| **Cambodia** | 20 | 35.0 | 30.0 | 85.0 | 100 | 95.0 | 75.0 | 15.0 |
| **Thailand** | **46** | | | **6.5** | **87** | **28.3** | **2.2** | **8.7** |
| **Nigeria** | 18 | 44.4 | 33.3 | 55.6 | 100 | 83.3 | 66.7 | 11.1 |

LA-ICP-MS analysis was used to compare the trace element chemistry of sapphires from other basalt-related deposits. Due to their similar geologic origin, plotting showed a large overlap. Some rough trends can be seen, but these are not conclusive. For example, a plot that shows Fe and Ga concentration, allows separation in large groups by Fe concentration (Figure 76):

- *Low Fe content between 500 and 1500 ppma*, suggests sapphire from Cambodia, Nigeria, blue sapphire from Thailand, and Australia (mostly Tasmania).
- *Medium Fe content between 1500 and 3500 ppma*, suggests blue sapphire from Thailand, and Australia (Queensland and New South Wales).
- *Fe content higher than 3500 ppma*, suggests greenish-blue sapphire from Thailand.

Note: Data from sapphires from other basalt-related deposits in Northern Madagascar, Cameroon, Kenya, China, Laos and Southern Vietnam are not included in this study yet.

Plotting between V and ratio of Ga/Mg showed overlapping between Thai blue sapphire and New South Wales and Queensland, Australia whereas Thai greenish blue sapphire can partially separate from others sources.

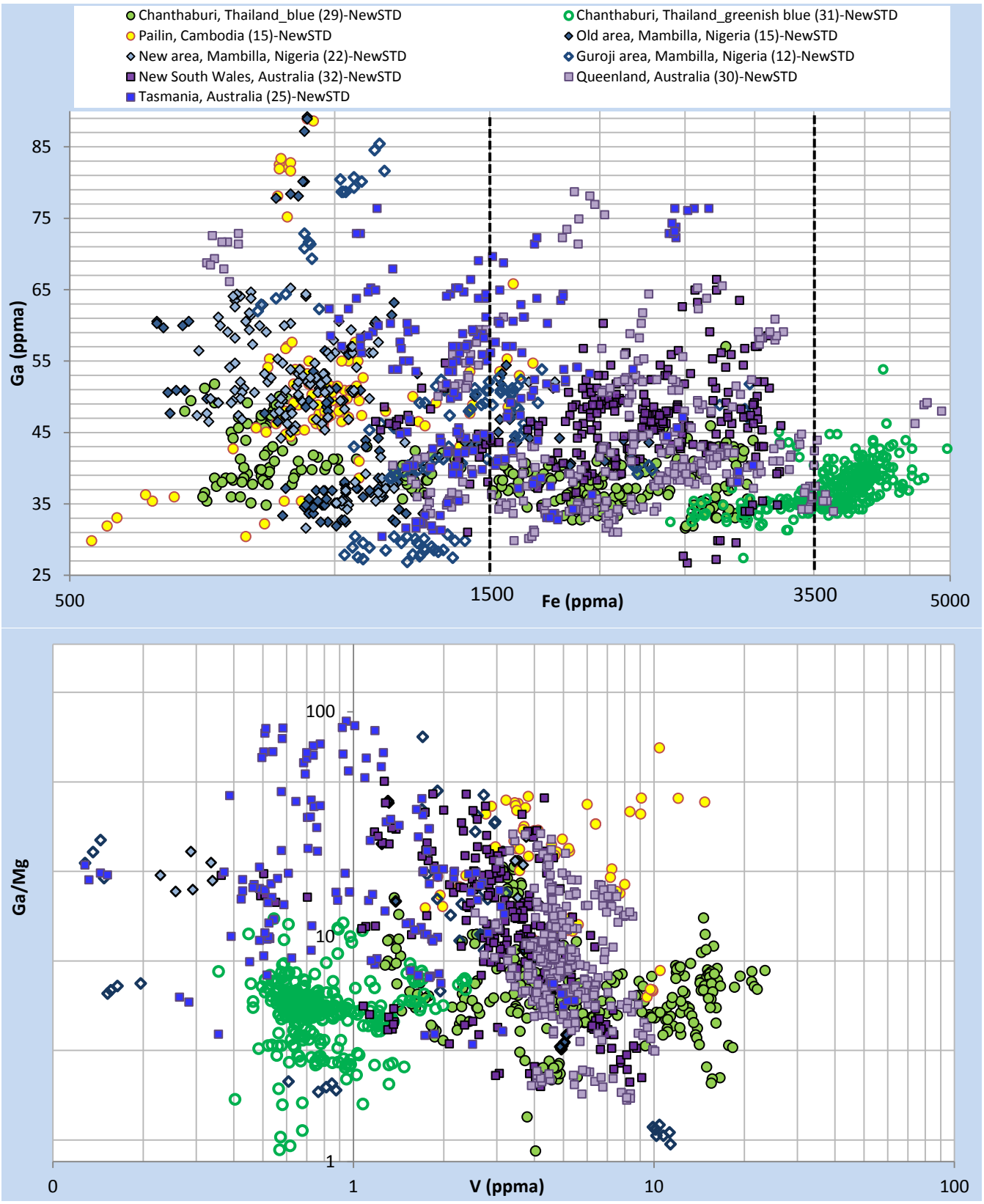


Figure 76: Plot showing Fe and Ga concentration (top) and V and ratio Ga/Mg (bottom) in sapphire samples from Chanthaburi-Trat, Thailand, compared to data from other basalt-related blue sapphire deposits in Australia, Cambodia, and Nigeria.

## PART IV. SUMMARY

Chanthaburi, Thailand commonly produces greenish blue, blue and yellow sapphire. The town serves as an active trading post, while the surrounding areas still have several active mines. Miners in this area often collaborate with farmers to mine farmland and later rehabilitate it. Thai sapphires are basalt related, similar to sapphires from Cambodia, Nigeria, Cameroon, Australia, Laos and Northern Madagascar. They formed deep below the earth's surface and were transported to the surface by alkali basalts. These have weathered in the Thai tropical climate and released the sapphires from the basalt matrix. This makes sapphire mining much easier, both on small and large scales.

We analyzed 59 samples collected at the mines near Khao Ploy Waen or bought straight from the miners. At the GIA laboratory in Bangkok, we fabricated these samples to optimize them for microphotography, spectroscopic and chemical analysis. UV-Vis-NIR spectroscopy revealed high absorption around 840-800 nm in the near-infrared region, which is characteristic of basalt-related sapphires. $Fe^{3+}$ and $Fe^{2+}$-$Ti^{4+}$ are responsible for the yellow and blue color respectively. A combination of both chromophores creates a green sapphire. The most frequent FTIR feature in Thai sapphire was a single peak at 3309 $cm^{-1}$, found in up to 60% of the studied samples. Only three samples showed 3309 with 3367 and 3232 $cm^{-1}$ unlike FTIR in other basalt-related sapphires. Unfortunately FTIR couldn't be used to conclusively determine locality origin because the 3309 series can be altered by heat treatment.

Determining the country of origin of basalt-related blue sapphire is very complicated. However; using a combination of multiple techniques could be useful, for example chemistry and microscopy. If a sample has needle inclusions and Fe concentration lower than 1000 ppma, it is more likely from Thailand. Samples with similarity chemistry from localities like Cambodia and Nigeria commonly have a more milky appearance (Pardieu; 2014). To fully support origin determination, the relationship between inclusions, spectra and chemistry needs further analysis and study.

**ACKNOWLEDGEMENTS.** The authors acknowledge and thank Dr. John Emmett, Duncan Pay, Shane McClure, and Dr. Wasura Soonthorntantikul for their useful advice and support. We also thank Vincent Pardieu and his team for samples collection; Sasithorn Engniwat for photo calibration and Victoria Liliane Raynaud-Flattot for sample fabrication.

**ABOUT THE AUTHORS.** Sudarat Saeseaw (ssaeseaw@gia.edu) is senior manager of colored stone identification in GIA's Bangkok laboratory. Dr. Supharart Sangsawong (ssangsaw@gia.edu) is a research scientist. Wim Vertriest (wvertrie@gia.edu) is a field gemologist. Victoria Liliane Raynaud-Flattot, Ungkhana Atikarnsakul, Charuwan Khowpong and Vararut Weeramonkhonlert are analysts, all from GIA's Bangkok laboratory.

## PART V. BIBLIOGRAPHY


Bauer, M. (1904). *Precious Stones*. London, Charles Griffin and Co.

Black, J. S. (1896). "Journey round Siam." *The Geographical Journal* , 8 (5): 429–452.

Dubinsky E.V. and Emmett J.L. (2013), "The colors of corundum." *Gem Guide,* 32 (1): 1-11.

Emmett J.L., Scarratt K., McClure S.F., Moses T., Douhit T.R., Hughes R., Novak S., Shigley J.E., Wang W., Bordelon O., Kane R.E. (2003), "Beryllium diffusion of ruby and sapphire" *Gems & Gemology,* 39 (2): 84-135.

Ferguson J. and Fielding P. E. (1971), "The origins of the colours of yellow, green and blue sapphires." *Chemical Physics Letters,* **10**(3): 262-265.

Ferguson J. and Fielding P. E. (1972), "The origins of the colours of natural yellow, blue, and green sapphires." *Australian Journal of Chemistry*, **25**: 1371-1385.

Hughes R. W., Manorotkul W. and Hughes E.B. (2017), *Ruby and sapphire: a gemologist's guide*, 1st edition, RWH Publishing/Lotus Publishing, Thailand.

Hughes, R. W. (2014). "Pleochroism in faceted gems: an introduction." *Gems & Gemology*, **50** (3): 216-226.

Groat, L. A. (Ed.) (2014). *Geology of Gem Deposits* (Second edition ed. Vol. Short Course Series, vol 44. Québec: Mineralogical Association of Canada.

Kammerling, R. C. (1990). "Gem News: Update on sapphire mining in Kanchanaburi." *Gems & Gemology*, 26 (4): 302-303.

Krebs J. J. and Maisch W. G. (1971), "Exchange effects in the optical-absorption spectrum of $Fe^{3+}$ in $Al_2O_3$." *Physical Review B* **4**(3): 757-769.

Levinson, A. A. and F. A. Cook (1994). "Gem corundum in alkali basalt: Origin and occurrence." *Gems & Gemology*, 30 (4): 253–262.

Moon A. R., and Phillips M. R. (1991), "Defect clustering in H,Ti:α-Al2O3". *Journal of Physics and Chemistry of Solids,* 52: 1087-1099.

Pardieu, V., S. Sangsawong, J. Muyal, and N. Sturman. (2014), "Blue sapphires from the Mambilla Plateau, Taraba State, Nigeria". *GIA News from Research.* https://www.gia.edu/gia-news-research-nigerian-source-blue-sapphire

Pavitt, J. A. L. (1973). "Sapphire mining in Chantaburi (Thailand)." *Journal of Gemmology*, 13: 302–307.

Smith, C. P., Kammerling, R.C., Keller, A.S., Peretti, A., Scarratt, K.V., Khoa, N.D., Repetto, S., (1995). "Sapphires from southern Vietnam." *Gems & Gemology***, 31** (3): 168–186.

Saminpanya, S., Sutherland, F.L., (2011). "Different origins of Thai area sapphire and ruby, derived from mineral inclusions and co-existing minerals." *European Journal of Mineralogy*, 23: 683–694.

Soonthorntantikul, W., Vertriest, W., Raynaud-Flattot, V., etc. (2017). "An In-Depth Gemological Study of Blue Sapphires from the Baw Mar Mine (Mogok, Myanmar)." https://www.gia.edu/gia-news-research/blue-sapphires-baw-mar-mine-mogok-myanmar

Sutherland, F. L., Hoskin, P.W.O., Fanning, C.M., Coenraads, R.R., (1998). "Models of corundum origin from alkali basaltic terrains, a reappraisal." Contrib Mineral Petrol , 133: 356-372.

Warington Smyth, H. (1898). *Five Years in Siam—From 1891 to 1896*. New York, Scribner's.